

Sea Surface Salinity Variability in the Tropical Indian Ocean

Bulusu Subrahmanyam¹, V.S.N. Murty², and David M. Heffner¹

¹*Department of Earth and Ocean Sciences, University of South Carolina, Columbia, USA.*

²*National Institute of Oceanography Regional Center (Council of Scientific and Industrial Research),
Visakhapatnam, India*

Abstract

Argo profiles of temperature and salinity data from the north Indian Ocean have been used to address the seasonal and interannual variability of Sea Surface Salinity (SSS) and SSS Anomaly (SSSA) in 2 boxes from the eastern Equatorial Indian Ocean (EIO: 5°S-5°N, 90°-95°E) and Southeastern Arabian Sea (SEAS: 5°-9°N, 72°-76°E) and to compare with the HYbrid Coordinate Ocean Model (HYCOM) simulated SSS for the period from January 2002 to February 2007. The observational period covered one strong negative Indian Ocean Dipole Zonal Mode (IODZM) event in 2005 and a strong positive IODZM event in 2006. The Argo profiles in each box captured the impact of these IODZM events with a larger impact in the EIO box showing salting (positive SSSA, +0.9) during negative IODZM (November 2005) and freshening (negative SSSA, -0.6) during positive IODZM (November 2006). A band of positive (negative) SSSA occurs in the central EIO during negative (positive) IODZM event in 2005 (2006) under the influence of IODZM dynamics. The impact of IODZM event in the SEAS is more evident during boreal winter months. The observed anomalous eastward (westward) surface current contributed to the observed intense salting (freshening) during negative (positive) IODZM event in the EIO. Following the IODZM events, the East India Coastal Current (EICC) gets modulated through the propagation of downwelling/upwelling Kelvin Waves and further lead to the freshening/salting in the SEAS during boreal winter. These are well corroborated with the HYCOM simulations of SSS and currents. This study emphasizes that the HYCOM simulated salinity fields would be useful to provide rapid checks revealing either problems or successes in the satellite retrievals of salinity from the Soil Moisture and Ocean Salinity (SMOS) and Aquarius missions.

Key words: Indian Ocean, Salinity, HYCOM, Argo and Indian Ocean Dipole Zonal Mode.

Corresponding Author:

Dr. Subrahmanyam Bulusu
Department of Earth and Ocean Sciences
701 Sumter Street, EWS 617
University of South Carolina
Columbia, SC 29208 USA

Tel: (803)-777-2572

Fax: (803)-777-6610

E-mail: sbulusu@geol.sc.edu

1. Introduction

There are many well-documented studies on the seasonal and interannual variability of Sea Surface Temperature (SST) in the tropical Indian Ocean from *in situ* observations, satellite measurements, and model simulations. [see the elaborate reviews by Schott and McCreary (2001); Annamalai and Murtugudde (2004); Schott *et al.*, 2009 and the numerous references therein]. The interannual variability in SST anomalies (SSTA) is interesting in the Equatorial Indian Ocean (EIO) wherein anomalous cooling (negative SSTA) occurs by October–November off the Sumatra coast in the eastern EIO and warming occurs in the western/central EIO, a phenomenon widely known as the positive IODZM event (Saji *et al.*, 1999; Webster *et al.*, 1999). During the negative IODZM event, the eastern EIO shows anomalous warming while the central/western EIO has negative SST anomalies (Saji *et al.*, 1999 and Rao *et al.*, 2002). Murtugudde and Busalacchi (1999), Murtugudde *et al.* (2000) and Rao *et al.* (2002) showed that the dynamics and thermodynamics and the associated circulation and subsurface variability are affected during the IOD years in the tropical Indian Ocean.

Compared to temperature measurements, salinity observations are sparse both temporally and spatially in the tropical oceans as there are no satellite salinity measurements as of now. However, based on the climatological salinity data (Conkright *et al.*, 2001) and sparse Sea Surface Salinity (SSS) data collected along Ships of Opportunity shipping lanes, the seasonal cycles of SSS have been studied to some extent in the tropical Indian Ocean (Donguy and Meyers, 1996; Rao and Sivakumar, 2003; Murty *et al.*, 2004 and Delcroix *et al.*, 2005). Modelers also used the available information on SSS variability for assessing numerical model performance (Murtugudde and Busalacchi, 1998) and for understanding climate variability (Murtugudde *et al.*, 2000).

With the launch of the Argo (Array for Real-time Geostrophic Oceanography) program, the number of temperature and salinity profiles repeated with 5/10 day cycles increased considerably in the tropical Indian Ocean (Anonymous, 2001) (visit <http://www.incois.gov.in> for more information). The Indian National Center for Ocean Information System (INCOIS), Hyderabad is the regional nodal agency for archiving the Argo profiles data gridded into 10-day cycles and 3°x3° boxes for the user community. Ravichandran *et al.* (2004) discussed the first results of India's Argo observations from SEAS highlighting the annual cycle of Argo SSS with lower SSS occurring in January–February and higher SSS during July–November. Shenoi *et al.* (2005) documented the evolution of SSS during March 2002–

April 2003 in the SEAS and reported that lower SSS waters first appeared in the eastern part of the SEAS during February-March 2003. Vinayachandran *et al.* (2005) noticed the bifurcation of EICC off east coast of Sri Lanka in non-IOD years and proposed that the low salinity waters from the Bay of Bengal may reach the SEAS through the Winter Monsoon Current (WMC). Gopalakrishna *et al.* (2005) studied SSS variability during 2002-05 and reported the occurrence of very low salinity waters in SEAS (the south box in their Figure 3c) during December 2003–February 2004. The continued SSS observations in the SEAS till June 2007 (Gopalakrishna, personal communication) showed considerable interannual variation in SSS with very low SSS (<33.0) in January–February 2004 and 2006 and relatively higher SSS (33.5 – 34.5) in February–March of 2003, 2005, and 2007. Phillips *et al.* (2005) examined the interannual variability of upper ocean salt content in the southeast Indian Ocean. Thompson *et al.* (2006) reported the Indian Ocean circulation and SSS variability during IODZM events, using different OGCM (Ocean General Circulation Model) simulations and assimilated data sets of SODA (Simple Ocean Data Assimilation) and ECCO (Estimating Climate and Circulation of the Ocean). They noted significant negative salinity anomalies in the central equatorial Indian Ocean (0–5°N; 75–90°E) during the positive IOD events. However, due to the lack of observations of long-term time-series salinity data in the tropical Indian Ocean, the interannual variability of salinity during the IODZM events is not completely documented.

The availability of long-term Argo profiles data motivated us to study the seasonal and interannual variability of observed Argo SSS and SSSA in relation to the IODZM events in two 5°x5° boxes selected in the eastern EIO and SEAS (Figure 1) during January 2002 – February 2007. The two selected boxes are located in the region of higher SSS variability in the eastern tropical Indian Ocean and help link the equatorial dynamics associated with the IODZM events and the observed interannual variability of SSS in the eastern EIO and SEAS. The Dipole Mode Index (DMI) data (<http://www.jamstec.go.jp>) for the study period suggests the occurrence of 2 positive IODZM events with cooler eastern EIO in the years 2003 and 2006. Rao *et al.* (2004) mentioned that the IODZM event in 2003 was intense in the June-September period and terminated early due to intraseasonal disturbances. The year 2005 was identified as a negative IODZM event with warm SSTs in the eastern EIO. Horri *et al.* (2008) reported that the year 2006 was a very strong positive IODZM event, with highest anomalous cooling (up to ~2°C) off southern Java coast in November 2006. Yoneyama *et al.* (2008), based on the MISMO (Mirai Indian Ocean cruise for the Study of the MJO-convection Onset) field Experiment in the central EIO (0°, 80.5°E) and the eastern EIO during October - December 2006,

highlight the presence of low salinity waters at 10 m depth in the central EIO (80.5°E) and their westward advection from the eastern EIO during the positive IODZM event in 2006 (Vinayachandran *et al.*, 2007). Anilkumar *et al.* (2007) also reported low salinity (<34.2) waters in the upper 40 m in the central EIO (77°-93°E) and their westward spread along the equator during September–October 2006, the period of positive IODZM event. McPhaden (2008) reported positive rainfall anomalies in the central EIO (80.5°E) in November 2006 in association with the positive IODZM 2006 event.

In this study, we have used the archived gridded Argo products (<http://www.incois.gov.in>, <http://www.coriolis.eu.org>) of temperature and salinity data in 3°x3° boxes and 10 day cycles for 5 year long-duration in the above selected boxes to understand the seasonal and interannual variability of SSS. This study has also prompted us to look into the performance of the high-resolution HYbrid Coordinated Ocean Model (HYCOM) simulations of SSS and currents in comparison with Argo SSS data during the IODZM events. River input and precipitation are also considered in the HYCOM simulations.

As the interannual variation of SSS is affected by the rainfall over the oceans, we have also examined the rainfall data (Adler *et al.*, 2003) obtained from Global Precipitation Climatology Project (GPCP) [<http://ftp.ncdc.noaa.gov/pub/data/gpcp/pentad/data>] in the selected boxes.

Section 2 gives a brief methodology of Argo data analysis and descriptions of HYCOM simulations. Section 3 describes results of the multi-year mean seasonal cycle and interannual variation of SSS and SSSA both from Argo and HYCOM data sets in each box. Section 4 provides discussion on the interrelationships between the SSSA variability in the two boxes and the linkage between the IODZM dynamics and the observed SSSA variability in the two boxes through the anomalous surface circulation derived from HYCOM simulations. Conclusions are given in Section 5.

It is expected that this study of comparison of Argo observed SSS with the HYCOM SSS fields would provide the necessary background to use the high resolution and wide-scale modeled salinity fields as a tool to compare and validate the satellite retrievals of SSS from the *SMOS* mission launched by the European Space Agency (ESA) and the *Aquarius* mission to be launched by National Atmospheric and Space Administration (NASA) and the Space Agency of Argentina (Comisión Nacional de Actividades Espaciales, CONAE). These missions would provide the first-ever global maps of sea surface salinity and offer the possibility of comprehensive SSS measurements.

2. Argo floats data and model simulations

2.1 Argo float data

Argo is a pilot programme of the Global Ocean Observing System. These data were collected and made freely available by the INCOIS and Coriolis project and the national programmes that contribute to it. The Argo Float mission was implemented in 1999 under the joint auspices of Climate Variability (CLIVAR) and Global Ocean Data Assimilation Experiment (GODAE), to produce unprecedented broad-scale measurements of temperature, salinity, and ocean circulation for climate and other applications. There are about 3175 Argo floats worldwide and 506 active floats in the Indian Ocean as of August, 2008 (<http://www-argo.ucsd.edu/>). Each Argo float is equipped to take salinity and temperature vertical profiles up to the parking depth of 2000 m. After 5/10 days of repeat cycle the float returns to the surface to transmit its position and data to a satellite, then returns to depth. The Argo salinity data in the upper 100 m from EIO box and SEAS box are compared with the collocated Conductivity-Temperature-Depth (CTD) salinity data at the stations in these boxes. In the SEAS, CTD (Seabird Electronics Inc., USA) temperature and salinity profiles were obtained as part of the Arabian Sea Monsoon Experiment (ARMEX) during 14 March – 10 April 2003 and 15 May – 19 June 2003 (Shenoi *et al.*, 2005) and during 15 April – 6 May 2005 (Murty *et al.*, 2006a). Coinciding with the period of the present study, there were two CTD salinity profiles in the SEAS box. Similarly, from the EIO box there was one CTD salinity profile in September 2006, obtained as part of the Ocean Observing System (OOS) program of the Ministry of Earth Sciences, Government of India.

In this study, we used the gridded Argo data product of 10 day interval in regular $3^{\circ}\times 3^{\circ}$ boxes archived at the Argo data center in INCOIS (<http://las.incois.gov.in>) in the north Indian Ocean from January 2002 to February 2007. Data at observation levels flagged in the Argo real-time quality control (e.g., spike check, density inversion check) were excluded. Float profiles with data from sparse vertical levels were also excluded in our analysis. The gridding was carried out based on a two-step interpolation method (Kessler and McCreary, 1993). In the first step, the T-S data from each profile were linearly interpolated to standard depths (i.e., 0, 10, 20, 30, 50, 75, 100, 125, 150, 200, 250, 300, 400, 500, 600, 700, 800, 900 and 1000 m), thereby creating a modified dataset. In the second step, the temperature and salinity of the modified dataset at each standard depth were mapped from irregular locations onto regular $3^{\circ}\times 3^{\circ}$ grids and 10-day timescales. The Argo float location changed slightly within the selected

box (EIO and SEAS) for each 10-day cycle over the study period, and this time variation of Argo profiles data was considered as 10-day interval time-series data from the selected boxes. Argo salinity at 5 m depth was taken as the Argo SSS. We extracted the Argo SSS data in the $5^{\circ}\times 5^{\circ}$ boxes located in the eastern EIO ($5^{\circ}\text{S}-5^{\circ}\text{N}$, $90^{\circ}-95^{\circ}\text{E}$) and SEAS ($5^{\circ}-9^{\circ}\text{N}$, $72^{\circ}-76^{\circ}\text{E}$) (Figure 1). The EIO box is further subdivided into EIO-north box ($2^{\circ}-5^{\circ}\text{N}$), EIO-equator box ($2^{\circ}\text{S}-2^{\circ}\text{N}$) and EIO-south box ($2^{\circ}-5^{\circ}\text{S}$) to examine the SSS and SSSA variability across the equator. From the original 10-day interval Argo SSS data, monthly mean Argo SSS data were obtained and the 5-year mean seasonal cycle was constructed for each box. The climatological monthly mean sea surface salinity data of the World Ocean Atlas of 2005 (WOA05) (Antonov *et al.*, 2006) in each box were also extracted for comparison with the monthly Argo SSS data in each box. The interannual Argo SSSA time-series in each box was obtained after removing the 5-year mean seasonal cycle of Argo SSS from monthly mean SSS in each year during 2002-06. In this study, for all the data sets, the seasonal cycle is defined as the time-variation of the monthly means of the parameter from January to December. The seasonal and interannual variability in Argo SSS and SSSA in each box are presented. The Argo SSS and SSSA are compared with the HYCOM simulated SSS and SSSA in the boxes for the study period 2002-2006.

2.2 HYCOM simulations

In this study we used global HYCOM with $1/12^{\circ}$ horizontal resolution and 32 hybrid layers in vertical. The model is configured on a Mercator grid from 78°S to 47°N , while north of this latitude an Arctic dipole patch is used to avoid the singularity at the pole. HYCOM was initialized using monthly mean temperature and salinity from the $1/4^{\circ}$ Generalized Digital Environmental Model (GDEM3) climatology (NAVOCEANO, 2003) in August. This experiment was then run for 13 years using climatological monthly mean wind and thermal forcing constructed from the 1.125° European Centre for Medium-Range Weather Forecasts (ECMWF) Re-Analysis (ERA15) over the 1979-1993 time frame. In addition, 6-hourly variability from the ECMWF operational model over the period September 1994 – September 1995 was added to the climatological wind forcing (but not the thermal forcing) to add the higher frequency variability needed for realistic simulation of the surface mixed layer. In order to keep the evaporation-precipitation budget on track, the model weakly relaxes to monthly mean SSS from the Polar Science Center Hydrographic Climatology (PHC) of Sea Surface Salinity. The actual SSS relaxation e-folding time depends on the mixed layer depth (MLD) ($30 \text{ days} \times 30 \text{ m} / \text{MLD m}$), i.e. it is more rapid when the MLD is shallow and less so when it is deep. The SSS relaxation is sufficient to

avoid long-term drift in SSS, but not so strong as to inhibit SSS anomaly formation. The SSS relaxation is in addition to the evaporation–precipitation budget.

Once the model was determined to be equilibrated after being spun-up with climatological forcing, the simulation was then continued using 3 hourly Navy Operational Global Atmospheric Prediction System (NOGAPS) winds, heat fluxes and precipitation fields for the period 2003-2006 as the forcing. This version of the model uses the NASA Goddard Institute for Space Studies (GISS) level 2 Mixed Layer scheme and includes monthly river runoff from 986 global rivers.

Daily HYCOM SSS simulations for the period January 2003 – December 2006 were used. We compared the HYCOM SSS at the collocated Argo float location at 10-day intervals with the Argo SSS during the observational period in each box (Figure 1) from the above 4 years period. HYCOM SSS data is extracted in the two 5°x5° boxes as described for Argo. While there is one Argo profile for every 10 days in each box, the HYCOM simulations are of 10 day averages over the box. Monthly mean HYCOM SSS data sets are obtained from the original daily HYCOM SSS data. Using the monthly HYCOM SSS data sets from each box, the 5 year-mean seasonal cycle of SSS is obtained for each box and interannual variation of HYCOM SSSA is obtained in a similar manner as Argo SSS analysis.

3. Results

3.1 Comparison of Argo salinity profiles with CTD salinity profiles

Figures 2a-b show the comparison of Argo salinity profiles with collocated CTD salinity profiles in the upper 100 m both in the SEAS and EIO boxes, and it is found that Argo data in the upper 30 m layer is consistent with the CTD salinity measurements. In the SEAS box, low salinity waters in the upper 20 m in April (Figure 2a) represent the seasonal variation (Ravichandran *et al.*, 2004). In the EIO box, very low salinity waters are noticed in the upper 30 m (Figure 2b) in September 2006 both in Argo salinity and CTD salinity profiles. The comparison shows smaller salinity differences in the upper 30 m, which are typically of the order of 0.1. This comparison, thus, gives confidence that Argo salinity profiles in each of EIO and SEAS boxes correctly captured the seasonal variations in sea surface salinity.

3.2 Climatological sea surface salinity in the eastern tropical Indian Ocean

Rao and Sivakumar (2003) discussed the seasonal variability of SSS in the tropical Indian Ocean using the comprehensive climatological data. Donguy and Meyers (1996) documented that the seasonal variation of SSS in the EIO is in part due to the seasonal variation of surface currents (Shankar *et al.*, 2002) in this region. Before proceeding further with the Argo salinity data analysis results, we present here the climatological (WOA05) SSS variation for the representative month of the seasons – January (winter monsoon), May (spring intermonsoon), July (summer monsoon) and October (fall intermonsoon) (Figures 3a-d). Both the river run-off into the Bay of Bengal and precipitation over the eastern tropical Indian Ocean (east of 65°E) are at minimum during spring intermonsoon (May), and are at their maximum during fall inter-monsoon (October) (Varkey *et al.*, 1996). Large seasonal variation can be seen in the northern and western Bay of Bengal and Andaman Sea and also in the SEAS (Delcroix *et al.*, 2005). In January, a high (34.8) salinity tongue is noticed south of Sri Lanka with salinity decreasing towards the Sumatra coast and SEAS (Figure 3a). In May, the low salinity waters in the SEAS show their persistence from winter months due to the advection of low salinity waters from the northern Bay of Bengal (Gopalakrishna *et al.*, 2005) through the equatorward EICC (Figure 3b). In July, the SSS is relatively high in the SEAS box from that of May (Figure 3c). Very low salinity waters occupy the western Bay of Bengal in October compared to May (Figure 3d). In October, high salinity waters occur in the SEAS box due to advection of Arabian Sea High Salinity waters from the northern Arabian Sea during summer monsoon (Shenoi *et al.*, 2005). In the EIO box (5°S-5°N; 90°-95°E), the SSS varies between 33.6 and 34.2 during both May and October. The WOA05 SSS climatology in October also suggests equatorward flow of very low salinity waters into the eastern Bay and into the eastern equatorial region (Figure 3d).

3.3 Interannual variation of rainfall in the selected boxes

Figure 4 presents the interannual variation of GPCP rainfall (mm/d) at the selected EIO box and SEAS box during January 2003 – February 2007. In the EIO box (5°S-5°N), the seasonal rainfall is high in the fall intermonsoon (September – November) and low in winter (January – April). The interannual variability in rainfall is highest (15 mm/d) in October 2005 and lowest (4 mm/d) in November 2006 and this variation is largely associated with the strong negative/positive IODZM events in 2005/2006. This is because during negative (positive) IODZM events, precipitation increases

(reduces) over the warmer (cooler) eastern EIO and decreases (increases) over the (cooler) warmer western and central EIO. Compared to the rainfall in the EIO box, the SEAS box receives slightly lower rainfall. In the SEAS box, the interannual variation in rainfall is also large in 2005 and 2006, unlike EIO, 2006 has larger variation than 2005. Since satellite rainfall estimates are known to underestimate rainfall over land, we have examined the observed all-India monthly mean rainfall data for the study period (2002-06) to understand its potential impact on the SSS variability in the western Bay of Bengal as the equatorward EICC would advect these waters into the SEAS. The all-India mean rainfall (data were downloaded from <http://www.iitm.res.in>) (Parthasarathy *et al.*, 1995) for the period June to September is relatively high in 2002 and 2004 and low in 2005 and the lowest in 2006 (Figure not shown). However, the all-India mean rainfall during October-December shows interestingly lower rainfall (350 – 500 mm) in 2002 and 2006 (again with dominant lowest rainfall in October) and relatively higher rainfall (~750-900 mm) during 2003-05 (with dominant highest rainfall in October). The highest (lowest) all-India mean rainfall in October 2005 (2006) coincides with the occurrences of higher (lower) GPCP rainfall in November 2005 (October 2006) over the western Bay of Bengal, and these well represent the respective negative (positive) IODZM events in 2005(2006). Thus the rainfall variations over the western Bay of Bengal during October-December 2005/2006 would impact the SSS variations along the east coast of India that would be advected into the SEAS through the equatorward EICC. In the following sections, we will show that the Argo SSSA in the SEAS box is affected following the IODZM events by the equatorward EICC from the western Bay of Bengal.

3.4 Seasonal and interannual variation of Argo SSS and model simulated SSS in the EIO

The EIO box (5°S-5°N and 90°-95°E) is further sub-divided into EIO-north box (2°-5°N), EIO-equator box (2°S-2°N) and EIO-south box (2°-5°S) to identify the SSS and SSSA variability across the equator. This sub-division emphasizes the occurrence of pronounced negative SSSA in the EIO-north box compared to that in the EIO-south box. The scatter plot between Argo SSS and HYCOM SSS at the collocated positions of floats at each 10 day cycle in the EIO box during the study period shows a linear positive relationship (Figure 5) with a high correlation coefficient ($r=0.61$) and HYCOM SSS is approximately higher by 0.5 from that of Argo SSS. The difference between the mean *rms* Argo SSS and the mean *rms* HYCOM SSS is -0.079 and the negative sign indicates that the overall observed Argo SSS values are lower than the HYCOM simulated SSS in the EIO box. The seasonal cycles of Argo SSS and WOA05 SSS in the entire EIO box are comparable, while the seasonal cycle of HYCOM SSS shows

lesser deviation from that of Argo SSS (Figure 6). All the three seasonal cycles show predominant semi-annual variation in SSS with two maxima occurring during November-January and May-June and two minima during March-April and September-October. This seasonal cycle of SSS in the EIO box is closely related to the seasonal cycle of rainfall over the EIO box (dashed curve in Figure 4) and also to the semi-annual variation of zonal currents advecting high/low salinity waters. However, the horizontal advection of low salinity waters from the eastern Bay of Bengal may also play a role in the interannual variability in SSSA in association with the intense positive/negative IODZM events.

Figures 7a-b represent the monthly variations of Argo SSS and SSSA during January 2002 – February 2007 in the EIO-north box, EIO-equator box and EIO-south box. The Argo SSSA in each box is obtained after removing the 5 years (2002-06) mean seasonal cycle of Argo SSS of each smaller box (Figure 7c). The seasonal cycle of SSS in the EIO-north box shows a large deviation from June to December with decreasing SSS, when compared to the seasonal cycles of SSS in the EIO-equator box and EIO-south box (Figure 7c). The seasonal cycle of the EIO-north box with minimum SSS of 33.55 in October (Figure 7c) affected the EIO-north box SSSA variation (Figure 7b). In the EIO-north box, lower (<33.8) SSS occurs during September – November and higher (34.5) SSS occurs in April-May (Figure 7a). The interannual variation in SSS in the EIO-north box is interestingly large with very low SSS occurring in October-November 2003 and September – December 2006 (Figure 7b), the periods of positive IODZM events. There is consistency in SSS variation between the EIO-equator box and EIO-south box. In the EIO-equator box, higher SSS occurs during November – December 2003, the period of fall equatorial jet and abrupt termination of the positive IODZM event (Rao *et al.*, 2004). However, in 2006, a freshening event (large decrease in SSS) took place in all boxes from April to December with very low salinity waters in the EIO-north box in November-December 2006 and in the EIO-equator box and EIO-south box in November (Figure 7b). The freshening event is less pronounced in the south box, due to westward advection of relatively high salinity waters from the southern Sumatra coastal upwelling region. The monthly variations of Argo SSSA in the boxes also registered the large freshening event with a reduction of SSSA by 1.5 (from +0.8 to -0.7) in the EIO-north box from November 2005 to November 2006. Similar drop in SSSA (from +0.2 to -1.0) is also seen in the EIO-equator box during the same period. We attribute this intense freshening event in the north box and reduced freshening in the south box to the dynamics associated with the development of an IODZM event in 2006. Earlier, Thompson *et al.* (2006) also reported large negative SSSA (up to -0.5) in the model simulations in the central EIO during the intense positive IODZM of 1997. This study shows that the Argo floats captured

the intense freshening event associated with the IODZM in 2006, which created a zonal salinity gradient in the equatorial region similar to the zonal SST gradient associated with the IODZM. We will discuss the intense freshening event in the following sections.

Figures 8a-d show the spatial variations of Argo SSSA during November 2003, 2004, 2005 and 2006. The November month is chosen as the representative period of peak IODZM development in the EIO region. A large negative SSSA occurs in the northern Bay and positive SSSA in the central Bay. Interannual variation in Argo SSSA is evident in the EIO region, SEAS and off the Sumatra coast. Development of large positive Argo SSSA (up to 1.0) in the SEAS and its eastward extent along the equator till 95°E is a noteworthy feature during negative IODZM event of November 2005 (Figure 8c). In November 2006, the period of strong positive IODZM event, one can see intense negative Argo SSSA (up to -1.0) in the eastern EIO with its southwestward extent from the Andaman Sea up to the south of Sri Lanka is evident (Figure 8d). Simultaneously, the Argo positive SSSA in the SEAS is reduced in magnitude and spatial extent. This contrasting variations in Argo SSSA in November 2005 and 2006 are also reflected in the HYCOM simulated SSSA variations (Figures not shown) suggesting that the latter are reasonable to address the interannual variation of SSS in the Indian Ocean.

3.5 Seasonal and interannual variation of Argo SSS and HYCOM SSS in the SEAS

The chosen box (5°-9°N, 72°-76°E) in the Arabian Sea is referred to as the SEAS box for simplicity. The present SEAS box (Figure 1) lies south of the usually christened SEAS (Shenoi *et al.*, 2005) and within the box of SSS observations denoted by “S” in Gopalakrishna *et al.* (2005, their Figure 1). The Winter Monsoon Current (WMC) during the boreal winter and the Summer Monsoon Current (SMC) during the boreal summer flow through the SEAS box (Shankar *et al.*, 2002).

The scatter plot between Argo SSS and the corresponding HYCOM SSS in the SEAS box (Figure 9) shows a good linear relation with a large correlation coefficient ($r = >0.79$). The difference between the mean *rms* Argo SSS and the mean *rms* HYCOM SSS is +0.144 and the positive sign indicates that the overall observed Argo SSS values are slightly higher than the HYCOM simulated SSS in the SEAS box. The scatter plot, however, shows two clusters, one on the low salinity side, and the other on high salinity side (Figure 9). The former represents the occurrence of low salinity waters during the boreal winter by advection through the EICC from the Bay of Bengal (Shenoi *et al.*, 2005; Gopalakrishna *et al.*, 2005; Durand *et al.*, 2007). However, there is also a possibility of advection of low salinity waters from the

eastern EIO as a source for the observed lower SSS in the SEAS. It is noteworthy to mention that Durand *et al.* (2007) suggested through numerical modeling studies that advection of the EICC contributes only about 30% of low salinity waters.

The seasonal cycle of Argo SSS coincides well with that of WOA05 SSS (Figure 10), but is on the higher side of the seasonal cycle of HYCOM SSS. It may be noted that the HYCOM SSS is just the surface value, while the Argo SSS is from 5 m below the surface. All the three seasonal cycles demonstrate annual variation of SSS (Figure 10) with lower SSS during boreal winter-spring (February-May) due to advection of low salinity waters of the Bay of Bengal by the EICC and possibly by WMC (Vinayachandran *et al.*, 2005), and their persistence. Higher SSS in October is due to the arrival of high salinity waters from the northern Arabian Sea and their persistence during July – November (Shenoi *et al.*, 2005).

The interannual variation of Argo SSS and HYCOM SSS during January 2002 – January 2007 demonstrates dominant annual variation of SSS in the SEAS (Figure 11a). The SSS drops sharply from 35.8 in early December 2005 to a minimum value of 33.9 in February 2006, with the arrival of low salinity waters from the Bay of Bengal through the equatorward EICC and possibly by WMC (Vinayachandran *et al.*, 2005) into the SEAS, since local rainfall is at minimum during January-April (Figure 4). This winter minimum Argo SSS value agrees with the SSS observations as reported in Gopalakrishna *et al.* (2005). One can notice an increase of SSS from February 2005 to a maximum SSS in August–September 2005. The interannual variation of Argo SSS (Figure 11a) and GPCP rainfall (Figure 4) during January 2003 – January 2007 in the SEAS box follow the same pattern; the period of minimum rainfall (January - April) coincides with that of minimum SSS. This suggests that the minimum SSS in the SEAS box is related to the advection of low salinity waters into the SEAS, as mentioned above. Similarly, though the rainfall in this area is high during the southwest monsoon, the SEAS experiences high salinity waters due to the advection of high salinity waters from the northern Arabian Sea through the equatorward flowing West India Coastal Current (Shenoi *et al.*, 2005). It is interesting to note that Argo SSS shows gradual freshening from 2002 to 2007 with a gradual reduction in the values of seasonal maximum (Figure 11a). The lowest winter minimum SSS (33.9) occurred in February 2006, subsequent to the negative IODZM event in 2005. HYCOM SSS shows a gradual increase in the values of seasonal maximum and minimum SSS, giving rise to large SSS differences in winter 2003 and weaker SSS differences in October 2006.

Figure 11b shows the interannual variation of Argo SSSA (obtained after removing the 5 year-mean seasonal cycle of Argo SSS) with a gradual decreasing trend in the Argo SSSA from the highest SSSA (0.8) in January 2002 to the lowest value (−0.8) in January-February 2006. From February 2006, the SSSA gradually increased till January 2007. The HYCOM SSSA, however, does show a little variation in SSSA during May 2005 – January 2007 (Figure 11b). Contrary to the dominant annual variation in the SSS in the SEAS (Figure 11a), its anomaly shows near semi-annual variation, suggesting a different mechanism for this variability.

4. Discussion

The study period (2002-2007) is dominated by the occurrence of positive and negative IODZM events of weaker to intense strength, as inferred from the DMI in SSTA (Saji *et al.*, 1999) data (<http://www.jamstec.go.jp>). The monthly variation of DMI for the study period (not shown here) shows positive SSTA ($>0.4^{\circ}\text{C}$) in November 2002, 2003 and November-December 2006, corresponding to positive IODZM events. Large negative SSTA ($<0.4^{\circ}\text{C}$) from October 2005 to February 2006 correspond to negative IODZM 2005. The impacts of strong negative IODZM event in 2005 and strong positive IODZM event in 2006 and the associated dynamics on the Argo SSSA variability during January 2002 - February 2007 in the EIO-north box and SEAS box are discussed in this section. The measured currents at the equator, 93°E , and the HYCOM simulations of currents and SSSA are used to understand the dynamics for the observed SSSA variability.

4.1 Zonal velocity and SSSA variability along the equator in the EIO box

The Acoustic Doppler Current Profiler (ADCP) measured currents in the upper 150 m at the equator, 93°E during November 2004 - June 2006, prior to the positive IODZM event in 2006 (Murty *et al.*, 2006, McPhaden *et al.*, 2009), are used to examine the monthly mean zonal velocity at 16 m depth during the period of observations (Figure 12). One can notice variability in the eastward flowing semi-annual equatorial jets - fall jets in November 2004 (18 cm/s) and October 2005 (22 cm/s) and spring jets in April 2005 (35 cm/s) and March 2006 (25 cm/s). Strengthening of the fall jet in 2005 and weakening of spring jet in 2006 can be associated with the negative (positive) IODZM events in 2005 (2006) respectively. Superposition of variation of monthly mean Argo SSSA from EIO-equator box on the monthly variation of zonal velocity at equator, 93°E shows that positive SSSA lags behind by 1-3 months from the occurrence of equatorial jets (Figure 12). Higher positive SSSA (0.48) occurs in April

2006 and thereafter drops rapidly to negative SSSA value. The eastward spring jet in 2006, however, weakens and reverses to westward flow from May to June followed by a decrease in SSSA from positive to negative value by June 2006. This westward flow advects low salinity waters leading to negative SSSA and represent the initial oceanic conditions in eastern EIO during the early development of IODZM in 2006 (Anilkumar et al., 2007, Yoneyama et al., 2008, Horri et al., 2008).

4.2 Interannual variation of Argo SSSA

The vertical structures of Argo salinity in the upper 200 m in the EIO-north box and EIO-equator box (Figures 13a-b) suggest interannual variability in the occurrence of low salinity waters both in depth and from the north box to equator box. Episodic events of thick (~40 m) layer of low salinity are noticed in the EIO-north box during July-December in 2003, 2004 and 2006.

The interannual variations of Argo SSSA in the EIO-north box and SEAS box are fitted with linear trend lines for the study period (Figure 14). The trend lines show decreasing trend in SSSA in the EIO-north box and SEAS box and the standard deviation (SD) of SSSA time-series in both the boxes is ± 0.28 . The length of time-series of Argo SSSA is, however, small (only 5 years) to draw the statistical significance of these trend lines. The negative trend lines representing freshening trend in the boxes draws one's attention. Steep freshening trend occurs in EIO-north box with a range of 0.66 (from +0.34 to -0.32), compared to gentle freshening trend with a range of 0.25 (from +0.15 to -0.10) in the SEAS box. Corresponding to the negative/positive IODZM events in 2005/2006 respectively, the interannual variation of Argo SSSA in the two boxes is large and opposite during 2005 and 2006. In the EIO-north box, a large positive SSSA (close to one SD) occurs during January – April 2005 and drops gradually to large negative SSSA by August 2005 due to increased rainfall (Figure 4) in association with the negative IODZM event of 2005. During the mature stage of negative IODZM in 2005, the observed SSSA in the EIO-north box rises steeply from negative SSSA in August to a peak positive (0.8) SSSA in November 2005 (Figure 14), at the time rainfall dropped to a lower value in the EIO-north box (Figure 4). Spatial variation of Argo SSSA also supports the presence of the band of positive SSSA in November 2005 (Figure 8) and during October – December 2005 (Figure 15). Interestingly, in 2006, negative Argo SSSA prevails from June to December 2006 in the EIO-north box with its peak value (-0.7, in excess of one SD) in November – December (Figure 14 and Figure 15e). At the same time, weaker negative SSSA is noticed in the SEAS box (Figure 14).

Figures 15a-e show the spatial variation of gridded Argo SSSA prior to (July-August), during (October – December) and after (January – February) the negative and positive IODZM events in 2005 and 2006 respectively. Prior to the negative IODZM event in 2005 (July-August) there occurs a band of negative SSSA along the equator in the eastern EIO and off northern Sumatra (Figure 15a). Off southern Sumatra coast, there occurs a weak positive SSSA. A large positive SSSA (+0.8) occurs in the SEAS and around Sri Lanka (Figure 15a). In the zonal belt of 10°S – 5°N, the bands of negative and positive SSSA are oriented in east-west direction. During the period of negative IODZM event, a band of higher positive (0.8) SSSA extends from the SEAS towards east along the equator and negative SSSA occurs around Sri Lanka (Figure 15b). Subsequent to the negative IODZM event, a large negative (-0.8 to -1.0) SSSA occupies the SEAS, a weak positive SSSA occupies the equatorial region and large positive SSSA occupies the western Bay of Bengal (Figure 15c). During the positive IODZM event in 2006 (October-December), large negative (-0.8) SSSA occurs in the equatorial region and a weak positive SSSA occurs both in the SEAS and off southern Sumatra (Figure 15e).

4.3 Interannual variation of HYCOM SSSA and surface circulation

Figures 16a-e show the maps of HYCOM simulations of mean SSSA (shaded) and mean current vector anomalies at sea surface for the periods prior to (July – August), during (October-December) and after (January-February) the IODZM events in 2005 and 2006. In these figures, the EIO-north box and SEAS box are depicted. The anomalies of SSS and current vectors are obtained after removing the respective 4 year (2003-06) mean seasonal cycles and the procedure followed is exactly the same as that for Argo SSS anomalies. The contrast in the anomalous circulation is more evident during and after the IODZM events (Figures 16b, c & e). The occurrence of a patch of positive (negative) SSSA in the central EIO during negative (positive) IODZM event in 2005 (2006) is noticed under the influence of the IODZM dynamics. The simulated SSSA and anomalous surface circulation patterns exhibit opposite variations during the IODZM events (Figures 16b&16e). The anomalous circulation features obtained from HYCOM simulations are in agreement with those from altimetric sea surface height anomaly maps (not shown). The eastward flowing fall equatorial jet during October-December 2005 (Figures 12 and 16b), anomalous westward flow along the equator during October – December 2006 (Figure 16e) and the anomalous EICC during these periods are associated with the negative/positive IODZM events in 2005/2006. During negative IODZM event in 2005, the anomalous surface circulation along the east coast of India is towards equator (Figure 16b) and in contrast, during the positive IODZM event in 2006,

it is poleward under the influence of coastally trapped upwelling Kelvin waves (Figure 16e). These anomalous circulation patterns are in agreements with that reported (Rao *et al.*, 2002, Thompson *et al.*, 2006).

During the negative IODZM event, strong anomalous westerly surface zonal winds prevail over the EIO and drive the eastward fall jet (Figure 12) that manifests in generation and eastward propagation of downwelling Kelvin Wave along the equator towards Sumatra coast. The fall jet advects high salinity waters from the western basin and gives rise to large positive Argo SSSA as observed in November 2005 (Figures 7b, 12, 14 and 15). Subsequent to the negative IODZM event in 2005, the SSSA in the EIO-north box falls to a weak positive value, the SEAS SSSA attains larger negative value (-0.7) by February 2006 (Figure 14), under the influence of both the westward flowing WMC from the southern Bay of Bengal (Figure 16c) and the flow of enhanced equatorward EICC advecting with it the low salinity waters of the northern Bay into the SEAS. The *in situ* salinity observations from the SEAS (Gopalakrishna, 2006, personal communication) support the large negative SSSA. Thus, the impact of the negative IODZM event in 2005 persists till the boreal winter season of 2006 in the SEAS.

On the contrary, during positive IODZM event anomalous easterlies blow over the eastern EIO and generate near-surface westward flow favoring equatorial upwelling (Rao *et al.*, 2002; Horii *et al.*, 2008) manifesting as an upwelling Kelvin wave in the eastern EIO. Vinayachandran *et al.* (1999), Rao *et al.* (2002) and Thompson *et al.* (2006) report that during positive IODZM event the fall equatorial jet (Wyrtki, 1973) is weakened and also the surface circulation in the Bay of Bengal during October-December is anomalously anticyclonic with a poleward flowing EICC along the east coast of India and an equatorward flow in the open-sea and Andaman Sea. During July – August 2006, prior to the development of the positive IODZM event, the pattern of anomalous surface circulation shows equatorward flow through the EIO-north box and a southeastward flow in the SEAS box (Figure 16d). During the mature stage of the positive IODZM event (October – December, 2006), the associated anomalous surface circulation shows an equatorward flow emanating from the Andaman Sea into the eastern EIO wherein a strong westward flow developed along the equator (Figure 16e) under the influence of anomalous easterly winds associated with the positive IODZM event (Vinayachandran *et al.*, 2007). In the core of the westward flow, the HYCOM SSSA is more negative between 75°E and 90°E and extends into the EIO-north box (Figure 16e). The spatial map of Argo SSSA during October – December 2006 also confirms the extensive negative SSSA region from the northern Sumatra coast in a

wide-band oriented southwestward across the equatorial region (Figure 15e). During the positive IODZM event, an upwelling equatorial Kelvin Wave is generated and propagates along the rim of Bay of Bengal and describes an anomalous anticyclonic circulation with a poleward flow along the east coast of India (Figure 16e). Subsequent to the positive IODZM event in 2006, the Argo SSSA variation is also changed (Figure 14) and is in tune with the change of patterns of surface circulation till January-February 2007 (not shown). The prevailing anomalous circulation suggests that low salinity waters from the Andaman Sea/Southern Bay of Bengal advect into the equatorial region during the positive IODZM, contributing to the negative SSSA in the EIO-north box and its westward spread into the central EIO (Figures 15e & 16e). This observation is in agreement with that of Thompson *et al.* (2006). Though the prevailing easterly winds during the positive IODZM in 2006 are favourable for coastal upwelling off northern Sumatra coast, one can notice the injection of low salinity waters from the Andaman Sea into the northern Sumatra coast (Figures 15e & 16e) and then along the equator into the EIO region. However, impact of coastal upwelling is seen off the southern coast of Sumatra at around 5°S, where higher positive Argo SSSA/HYCOM SSSA is noticed (Figures 15e & 16e) as the upwelled subsurface waters are of high salinity.

4.4 Time-longitude plot of HYCOM SSSA along 5°N latitude

The Hovmöller longitude-time plots of HYCOM SSSA (Figure 17) along 5°N reveals the propagation of bands of negative and positive SSSA in association with westward propagation of annual Rossby waves from eastern EIO up to SEAS modulating the surface salinity leading to SSSA in the SEAS box. In general, in the eastern EIO, the HYCOM SSSA at 5°N shows positive SSSA in April-May and negative SSSA in September – December. In the SEAS, negative SSSA occurs during January - February and positive SSSA during September-October. During the positive IODZM event in 2006, the SSSA is more negative (-0.8 to -1.0) in the eastern EIO during October – December 2006. The phase lines (shown by bold straight lines) connecting the positive SSSA/ negative SSSA show that the sea surface salinity in the SEAS is also affected by the salinity variations in the eastern EIO that are propagated by the Rossby Waves during the anomalous climatic events such as the Indian Ocean Dipole Mode.

5. Conclusions

The gridded Argo profiles data onto $3^{\circ} \times 3^{\circ}$ grids in 10 day cycles during January 2002 – February 2007 from two $5^{\circ} \times 5^{\circ}$ boxes located in the eastern EIO and SEAS are analyzed to address the seasonal SSS and interannual variation of SSS anomalies (obtained after subtracting the multi-year mean seasonal cycle) in these boxes in relation to the positive/negative IODZM events in 2005 and 2006. The high resolution HYCOM simulations of SSS and surface currents during 2003-06 are used to understand the dynamics behind the interannual variability of SSSA. The mean seasonal cycles of Argo SSS, HYCOM SSS and the climatological WOA05 SSS are compared in both the boxes and found that HYCOM simulated salinity is underestimated.

During the negative IODZM event in 2005, positive Argo SSSA occurred in the EIO-north box (2° - 5° N, 90° - 95° E) during October – December 2005 and during the positive IODZM event in 2006 large negative Argo SSSA during October – December 2006 occurred in the same EIO-north box. Simultaneously, weaker magnitude of similar type SSSA occurred in the SEAS in each case of IODZM event. This is substantiated from the interannual variability of Argo SSSA and from HYCOM simulated SSSA and surface currents. It is also found that the interannual variability in the Argo SSSA/HYCOM SSSA in the SEAS is affected by the interannual variability in the eastern EIO through the westward propagation of Rossby Waves, and also from the interannual variability in the equatorward flowing seasonal EICC that affected during the IODZM events.

During the positive IODZM event of 2006, anomalous equatorward flow emanates from the Andaman Sea and advects low salinity waters into the EIO, thus large negative SSSA (freshening) is developed in the EIO. This large negative SSSA is further advected westward through the anomalous westward flow (Figure 16e) to the central EIO. At the same time, the seasonal EICC weakened with the anomalous poleward flow and contributes to reduction in the negative SSSA by the following boreal winter months. The same dynamics work even during negative IODZM events, but contribute to more negative SSSA in the SEAS during winter months (Figure 8d) following the negative IODZM event, through the strengthened equatorward EICC.

This study further indicates that the linear trend lines fitted to the interannual variation of SSSA in the EIO-north box (2° N- 5° N) and SEAS box reveal an interesting feature of freshening (decreasing trend

line of SSSA) in both EIO box and SEAS box, with higher freshening trend in the latter over the period of Argo observations used in this study.

This important observation together with the salt budget of the region needs further study with SMOS and Aquarius Salinity missions, more Argo data sets and model simulations. We will take up this study in our future work.

Acknowledgements

Bulusu Subrahmanyam and David Heffner were partially supported by the NASA Physical Oceanography Program under Grant# NNG06GJ22G awarded to BS. VSNM, is thankful to the Director of NIO and to his students who helped him in this study at various stages during their stay at NIO. Horri Takanori, JAMSTEC, Japan provided the time series of Dipole Mode Index (DMI) data. The HYCOM model results were provided by Dr. Jay Shriver, Naval Research Laboratory, Stennis Space Center, MS. The gridded Argo data were collected and made freely available by the International Argo Project and the national programmes that contribute to it (<http://www.argo.ucsd.edu> , <http://www.incois.gov.in>, <http://argo.jcommops.org>, <http://www.coriolis.eu.org>). We gratefully acknowledge useful suggestions from the reviewers. This has the NIO Contribution No. xxxxx

References

- Adler RF, Huffman GJ, Chang A, et al., 2003, The Version-2 Global Precipitation Climatology project (GPCP) monthly precipitation analysis (1979-present), *J. Hydrometeor.*, **4** (6), 1147-1167.
- Anilkumar M, Murty VSN, Sarma MSS, Lakshmi ASN, Vidya PJ, Almeida A, Charyulu RJK (2007) Upper ocean observations in the equatorial Indian Ocean during 2004-06 (abstract). Presented at the Ocean Science Session (OS-17) of the Asia Oceania Geosciences Society (AOGS-2007) conference held in Bangkok, Thailand during 31 July – 4 August 2007.
- Annamalai H, Murtugudde R, Potemra J, Xie SP, Liu P, Wang B (2003) Coupled dynamics over the Indian Ocean: Spring initiation of the zonal mode. *Deep Sea Research Part II* 50: 2305– 2330.
- Annamalai H, Murtugudde R (2004) Role of the Indian Ocean in regional climate variability. In *Earth Climate: The Ocean-Atmosphere Interaction*, C. Wang, S.-P. Xie and J.A. Carton (eds.), *AGU Geophysical Monograph*, 147, 213–246.
- Anonymous (2001) Report of the Indian Ocean Argo Implementation Planning Meeting, Indian National Centre for Ocean Information System (INCOIS), Hyderabad, India.

- Antonov JI, Locarnini RA, Boyer TP, Mishonov AV, and Garcia HE (2006) World Ocean Atlas 2005, Volume 2: Salinity. S. Levitus, Ed. NOAA Atlas NESDIS 62, U.S. Government Printing Office, Washington, D.C., 182 pp.
- Babu MT, Sarma YVB, Murty VSN, and Vethamony P (2003) On the circulation in the Bay of Bengal during northern spring inter-monsoon (March–April 1987). *Deep-Sea Research Part II: Topical Studies in Oceanography* 50: 855–865.
- Conkright ME, O’Brien TD, Boyer TP, Stephens C, Locarnini RA, Garcia HE, Murphy PP, Johnson D, Baranova O, Antonov JI, Tatusko R, Gelfeld R, Smolyar I, (2001) *World Ocean Database 2001, CD-ROM Data Set Documentation*. National Oceanographic Data Center, Silver Spring, MD, 137 pp, 2001.
- Delcroix T, Dessier A, Gourriou Y, McPhaden M (2005) Time and space scales for sea surface salinity in the tropical oceans. *Deep-Sea Research* 52: 787-813.
- Donguy JE, Meyers G (1996) Seasonal variations of sea surface salinity and temperature in the tropical Indian Ocean. *Deep-sea Research* 43: 117-138.
- Durand F, Shankar D, de Boyer Montégut C, Shenoi SSC, Blanke B, and Madec G (2007) Modelling the barrier-layer formation in the South-Eastern Arabian Sea. *Journal of Climate* 20: doi: 10.1175/JCLI4112.1.
- Gopalakrishna VV., Johnson Z, Salgaonkar G, Nisha K, Rajan CK, Rao R.R (2005). Observed variability of sea surface salinity and thermal inversions in the Lakshadweep Sea during contrast monsoons. *Geophysical Research Letters* 32: doi:10.1029/2005GL023280.
- Heffner, DM, Subrahmanyam B, Shriver JF (2008). Indian Ocean Rossby waves detected in HYCOM sea surface salinity. *Geophysical Research Letters* 35, doi:10.1029/2007GL032760.
- Horri T, Hase H, Ueki I, Masumoto Y (2008). Oceanic precondition and evolution of the 2006 Indian Ocean Dipole. *Geophysical Research Letters* 35: doi:10.1029/2007/GL032464.
- Jochum M, Murtugudde R (2005). Internal variability of Indian Ocean SST. *Journal of Climate* 18: 3726– 3738.
- Kessler WS, McCreary JP (1993). The Annual Wind-driven Rossby Wave in the Subthermocline Equatorial Pacific. *Journal of Physical Oceanography* 23: 1192- 1207.
- Kumar SP, Unnikrishnan AS, Muraleedharan PM (2000). Signatures of Kelvin and Rossby wave propagation in the northern Indian Ocean from TOPEX/Poseidon altimeter. PORSEC Proceedings, Vol. I, 276-279, held in Goa, India, December 5-8, 2000.

- Lagerloef GSE, Swift CT, LeVine DM (1995). Sea surface salinity: the next remote sensing challenge. *Oceanography* 8: 44-50, 1995.
- McCreary JP, Kundu PK, Molinari RL (1993). A numerical investigation of dynamics, thermodynamics and mixed layer processes in the Indian Ocean. *Progress in Oceanography* 31: 181-244.
- McPhaden MJ (2008). Evolution of the 2006-07 El Niño: The Role of Intraseasonal to Interannual Time Scale Dynamics. *Advanced Geosciences* 14: 219-230.
- McPhaden MJ, Meyers G, Ando K, Masumoto Y, Murty VSN, Ravichandran M, Syamsudin F, Vialard J, Yu L, Yu W (2009). RAMA The Research Moored Array for African – Asian – Australian Monsoon Analysis and prediction. *Bull. Am. Meteorol. Soc.*, 90(4), 459-480.
- Murtugudde R, Busalacchi A (1998). Salinity effects in a tropical ocean model. *Journal of Geophysical Research* 103: 3283-3300.
- Murtugudde R, Busalacchi A (1999). Interannual variability of the Dynamics and Thermodynamics of the tropical Indian Ocean. *Journal of Climate* 12: 2300-2326.
- Murtugudde R, Signorini S, Christian J, Busalacchi A, McClain C (1999). Ocean color variability of the tropical Indo-Pacific basin observed by SeaWiFS during 1997 – 1998 *Journal of Geophysical Research* 104: 18,351–18,366.
- Murtugudde R, McCreary JP, and Busalacchi AJ (2000). Oceanic processes associated with anomalous events in the Indian Ocean with relevance to 1997-1998, *Journal of Geophysical Research* 105: 3295-3306.
- Murty VSN, Sarma YVB, Rao DP, Murty CS (1992). Water characteristics, mixing and circulation in the Bay of Bengal during southwest monsoon. *Journal of Marine Research* 50: 207-228.
- Murty VSN, Subrahmanyam B, Tilvi V, O'Brien JJ (2004). A new technique for the estimation of sea surface salinity using the Outgoing Longwave Radiation. *Journal of Geophysical Research* 109: doi:10.1029/2003JC001928.
- Murty VSN, Murali Krishna S, Nagaraju A, Somayajulu YK, Ramesh Babu V, Sengupta D, Sindu PP, Ravichandran M, Rajesh G (2006a). On the warm pool dynamics in the southeastern Arabian Sea during April – May 2005 based on the satellite remote sensing and ARGO float data. *Proceedings of SPIE volume 6406: Remote Sensing of the Marine Environment*, (eds.) Robert J. Frouin, Vijay K. Agarwal, Hiroshi Kawamura, Shailesh Nayak, Delu Pan. Available at <http://drs.nio.org/drs/handle/2264/548>.

- Murty VSN, Sarma MSS, Suryanarayana A, Sengupta D, Unnikrishnan AS, Fernando V, Almeida A, Khalap S, Sardar A, Somasundar K, Ravichandran M (2006b). Indian Moorings: Deep-sea current meter moorings in the Eastern Equatorial Indian Ocean, *CLIVAR-Exchanges*, No. 39, vol. 11, No. 4, 5-8.
- NAVOCEANO, 2003: Database description for the generalized digital environmental model (GDEM--V) Version 3.0. OAML--DBD--72, 34~pp. [Available from NAVOCEANO Oceanographic Data Bases Division, Stennis Space Center, MS 39522--5001.]
- Parthasarathy B, Munot AA, Kothawale DR (1995) All India monthly and seasonal rainfall series : 1871-1993. *Theor. and Appl. Climatol.*, 49, 217-224.
- Pearson ES, Hartley HO (1976). *Biometrika Tables for Statisticians*, Cambridge Univ. Press (Sd); 3rd edition, 286.
- Phillips HE, Wijffels SE, Feng M (2005). Interannual variability in upper ocean salt content in the southeast Indian Ocean. *Geophysical Research Letters* 32: doi:10.1029/2004GL021755.
- Rao SA, Behera SK, Masumoto Y, Yamagata T (2002). Interannual subsurface variability in the tropical Indian Ocean with a special emphasis on the Indian Ocean Dipole. *Deep Sea Research* 49: 1549-1572.
- Rao RR, Sivakumar R (2003). Seasonal variability of sea surface salinity and salt budget of the mixed layer of the north Indian Ocean. *Journal of Geophysical Research* 108: doi:10.1029/2001JC000907.
- Rao AS, Yamagata T (2004). Abrupt termination of Indian Ocean dipole events in response to intraseasonal disturbances. *Geophysical Research Letters* 31: doi:10.1029/2004GL020842,
- Rao AS, Yamagata, T (2004). Abrupt termination of Indian Ocean dipole events in response to intraseasonal disturbances. *Geophys. Res. Lett.*, 31, L19306, doi:10.1029/2004GL020842.
- Ravichandran M, Vinayachandran PM, Joseph S, Radhakrishnan K (2004). Results from the first Argo float deployed by India. *Current Science* 86: 651-659.
- Reynolds RW, Rayner NA, Smith TM, Stokes DC, Wang W (2002). An improved in situ and satellite SST analysis for climate. *Journal of Climate* 15: 1609-1625.
- Saji NH, Goswami BN, Vinayachandran PN, Yamagata T (1999). A dipole mode in the tropical Indian Ocean. *Nature* 401: 360-363.
- Schott F, McCreary JP(2001). The monsoon circulation of the Indian Ocean. *Progress in Oceanography* 51: 1-123.

- Schott FA, Xie Shang-Ping and McCreary JP (2009) Indian Ocean circulation and climate variability. *Rev. Geophys*, 47, RG1002, 46.
- Seager R, Murtugudde R (1997). Ocean Dynamics, Thermocline Adjustment, and Regulation of Tropical SST. *Journal of Climate* 10: 521–534.
- Sengupta D, Bharath Raj GN, Shenoi SSC (2006). Surface freshwater from Bay of Bengal runoff and Indonesian Throughflow in the tropical Indian Ocean, *Geophysical Research Letters* 33: doi:10.1029/2006GL027573.
- Shankar D, McCreary JP, Han W, Shetye SR (1996). Dynamics of the East India Coastal Current: Part 1, analytic solutions forced by interior Ekman pumping and local alongshore winds. *Journal of Geophysical Research* 101: 975-13,991.
- Shankar D, Vinayachandran PN, Unnikrishnan AS (2002). The monsoon currents in the north Indian Ocean. *Progress in Oceanography* 52: 63-120.
- Shenoi SC, Shankar D, Gopalakrishna VV, Durand F (2005). Role of ocean in the genesis and annihilation of the core of the warm pool in the southeastern Arabian Sea. *Mausam* 56: 147-160.
- Shetye SR, Shenoi SSC, Gouveia AD, Michael GS, Sundar D, Nampoothiri G (1991), Wind-driven coastal upwelling along the western boundary of the Bay of Bengal during the southwest monsoon. *Continental Shelf Research* 11: 1397-1408.
- Subrahmanyam, B. , D.M. Heffner, D. Cromwell, J.F. Shriver, (2009). Detection of Rossby Waves in Multi-parameters in Multi-mission Satellite Observations and HYCOM simulations in the Indian Ocean, *Remote Sensing of Environment*, 113, 1293-1303.
- Thompson, B, Gnanaseelan, C, Salvekar, PS (2006). Variability in the Indian Ocean circulation and salinity and its impact on SST anomalies during dipole events. *J. Mar. Res.*, 64, 853-880.
- Varkey MJ, Murty VSN, Suryanarayana A (1996). Physical Oceanography of the Bay of Bengal and Andaman Sea. *Oceanography and Marine Biology: an Annual Review* 34:1-70. A. D. Ansel, R. N. Gibson and Margaret Barnes (Eds.), UCL Press.
- Vinayachandran, PN, Saji, NH and Yamagata, T (1999) Response of the Equatorial Indian Ocean to an unusual wind event during 1994. *Geophys. Res. Lett.*, 26,11, 1616-1619.
- Vinayachandran PN, Murty VSN, Ramesh Babu V (2002). Observation of barrier layer formation in the Bay of Bengal during summer monsoon. *Journal of Geophysical Research* 107: doi:10.1029/2001JC000831.

- Vinayachandran PN, Kagimoto T, Masumoto Y, Chauhan P, Nayak SR, and Yamagata T (2005). Bifurcation of the East India Coastal Current east of Sri Lanka. *Geophysical Research Letters* 32: doi:10.1029/2005GL022864.
- Vinayachandran PN, Kurian J, Neema CP (2007). Indian Ocean response to anomalous conditions in 2006. *Geophysical Research Letters* 34: doi:10.1029/2007GL030194.
- Waliser DE, Murtugudde R, Lucas LE (2004). Indo-Pacific Ocean response to atmospheric intraseasonal variability: 2. Boreal summer and the Intraseasonal Oscillation, *Journal of Geophysical Research* 109: doi:10.1029/2003JC002002
- Webster PJ, Moore AM, Loschnigg JP, Leben RR (1999). Coupled ocean-atmosphere dynamics in the Indian Ocean during 1997-98. *Nature* 401: 356-360.
- Wiggert JD, Murtugudde RG, Christian JR (2006). Annual ecosystem variability in the tropical Indian Ocean: Results of a coupled bio-physical ocean general circulation model. *Deep Sea Research* 53: 644-676.
- Wiggert JD, Murtugudde RG (2007). The sensitivity of the southwest monsoon phytoplankton bloom to variations in aeolian iron deposition over the Arabian Sea. *Journal of Geophysical Research* 112: doi:10.1029/2006JC003514.
- Wyrtki K (1973). An equatorial jet in the Indian Ocean. *Science* 181: 262-264.
- Yoneyama K, Masumoto Y, Kuroda Y, Katsumata M, Mizuno K, Takayabu YN, Yoshizaki M, Shareef A, Fujiyoshi Y, McPhaden MJ, Murty VSN, Shirooka R, Yasunaga K, Yamada H, Sato N, Ushiyama T, Moteki Q, Seiki A, Fujita M, Ando K, Hase H, Ueki I, Horii T, Yokoyama C, and Miyakawa T (2008). MISMO Field Experiment in the Equatorial Indian Ocean. *Bulletin of American Meteorological Society*, **89**, 1889- 1903, doi:10.1175/2008BAMS2519.1
- Yu L, O'Brien JJ, and Yang J(1991). On the remote forcing of the circulation in the Bay of Bengal. *Journal of Geophysical Research* 96: 20449-20454.

Figure Captions

- Figure 1 Study area showing the boxes in the Equatorial Indian Ocean (EIO: 5°S - 5°N and 90° - 95°E) and Southeastern Arabian Sea (SEAS: 5°-9°N, 72°-76°E). The EIO box is further divided into EIO-north box, EIO-equator box and EIO-south box.
- Figure 2 Comparison of *in situ* CTD salinity profiles (triangle) with the collocated Argo salinity profile (Asterix) in the (a) SEAS box and (b) EIO-equator box. The CTD data were collected during Arabian Sea Monsoon Experiment (ARMEX) closer to the SEAS box and the Ocean Observing System (OOS) Current meter mooring surveys in the EIO-equator box.
- Figure 3. World Ocean Atlas 2005 (WOA05) climatological Sea Surface Salinity (SSS) during (a) January, (b) May, (c) July, and (d) October.
- Figure 4. Interannual variation of rainfall obtained from the Global Precipitation Climatology Project (GPCP) in the EIO and SEAS during January 2003-February 2007.
- Figure 5. Scatter plot of Argo SSS and HYCOM SSS in the EIO box. The HYCOM output was obtained at each location of the 10 day cycle Argo float (s) in the EIO box during 2003-06. The correlation coefficient (r) between Argo SSS and HYCOM SSS is 0.61.
- Figure 6. Annual variations of climatological (WOA05) SSS, Argo SSS and HYCOM SSS in the EIO box. The seasonal cycle of Argo SSS is based on the data from January 2002 to December 2006 (5 years) and that of HYCOM SSS is based on data from January 2003 to December 2006 (4 years).
- Figure 7. Interannual variation of (a) Argo SSS, (b) Argo SSS Anomaly during January 2002 – February 2007 and (c) annual cycles of Argo SSS in each of the Equatorial boxes [EIO-north box, EIO-equator box and EIO-south box]. The 5 year mean (2002-06) seasonal cycle (12 months) of Argo SSS (c) for each box is removed to obtain the Argo SSS Anomaly in each box.
- Figure 8. Spatial variations of monthly mean Argo SSSA for November in different years in the tropical Indian Ocean during (a) 2003, (b) 2004, (c) 2005 and (d) 2006.
- Figure 9. Scatter plot of Argo SSS and HYCOM SSS in the SEAS box. The HYCOM SSS output is obtained at each location of the 10 day cycle Argo float(s) in the SEAS box during May 2004 - October 2005. The correlation coefficient (r) between Argo SSS and HYCOM SSS is 0.79.

- Figure 10. Annual variations of climatological (WOA05) SSS, Argo SSS and HYCOM SSS in the SEAS box.
- Figure 11. Interannual variations of (a) Argo SSS and HYCOM SSS, and (b) Argo SSSA and HYCOM SSSA in the SEAS box during January 2002-January 2007.
- Figure 12. Acoustic Doppler Current Profiler (ADCP) measured monthly mean zonal velocity (cm/s) at 16 m depth (solid line) at 0° , 93° E and Argo SSSA (dashed line) in the EIO-equator box during November 2004 – July 2006.
- Figure 13. Interannual variation of Argo Salinity structure in the upper 200 m in the (a) EIO-north box (2° N- 5° N, 90° - 95° E) and (b) EIO-equator box (2° S- 2° N, 90° - 95° E) during 2002-2006.
- Figure 14. Interannual variation of Argo SSSA in the EIO-north box and SEAS box during January 2002 – February 2007. Standard deviation for both data sets is the same and is shown by horizontal lines. Linear trend lines fitted for SSSA variation in each box are also shown.
- Figure 15. Spatial variation of gridded Argo SSSA (obtained after subtracting the 5 year (2002-2006) mean seasonal cycle) for the selected periods (a & d) prior to IODZM event (July-August), (b & e) during the IODZM event (October – December), (c) after the negative IODZM event (January – February 2006).
- Figure 16. HYCOM simulations of Sea Surface Salinity Anomaly (color shading) and current vectors anomaly for the selected periods of (a & d) prior to IODZM event (July-August), (b & e) during the IODZM event (October – December), (c) after the negative IODZM event (January – February 2006). The 4 years (2003-2006) mean seasonal cycle is subtracted to obtain the anomalies in the model surface salinity and surface currents.
- Figure 17. Longitude-Time plot of HYCOM SSSA in the southern Bay of Bengal along 5° N latitude during 2003-2006.

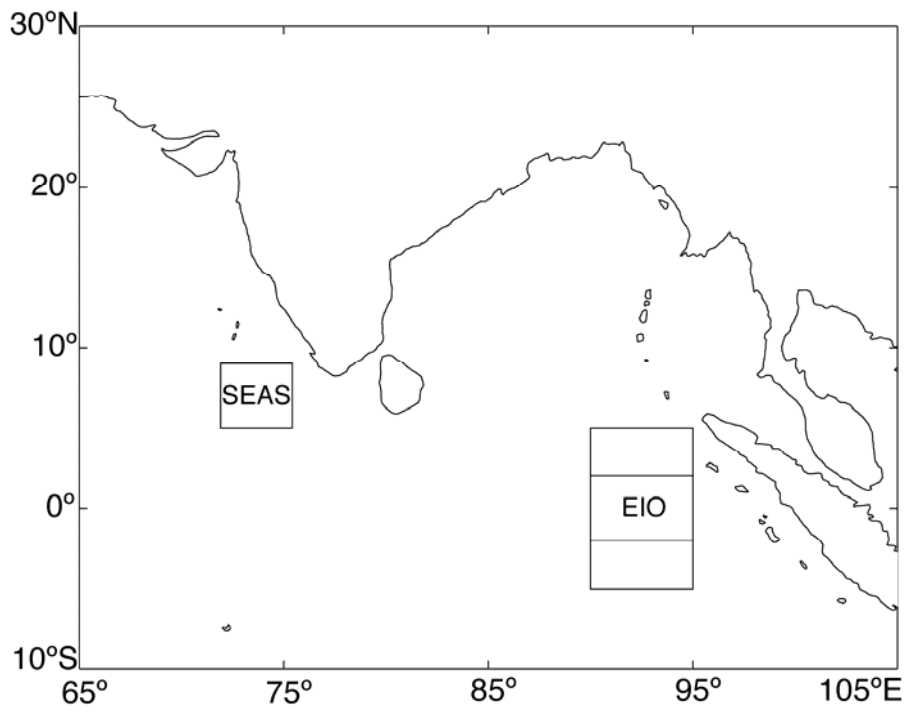


Figure 1. Study area showing the boxes in the Equatorial Indian Ocean (EIO), Southeastern Arabian Sea (SEAS), and Bay of Bengal (BoB).

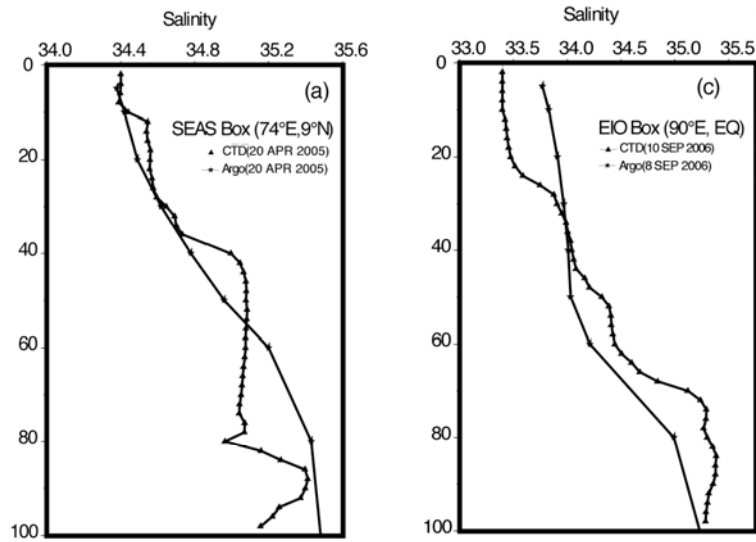


Figure 2. Comparison of in situ CTD salinity profiles (triangle) with the collocated Argo salinity profile (Asterix) in the (a) SEAS box (b) EIO-equator box. The CTD data were collected during the Arabian Sea Monsoon Experiment (ARMEX) closer to the SEAS box and the Ocean Observing System (OOS) current meter mooring surveys in the EIO-Equator box.

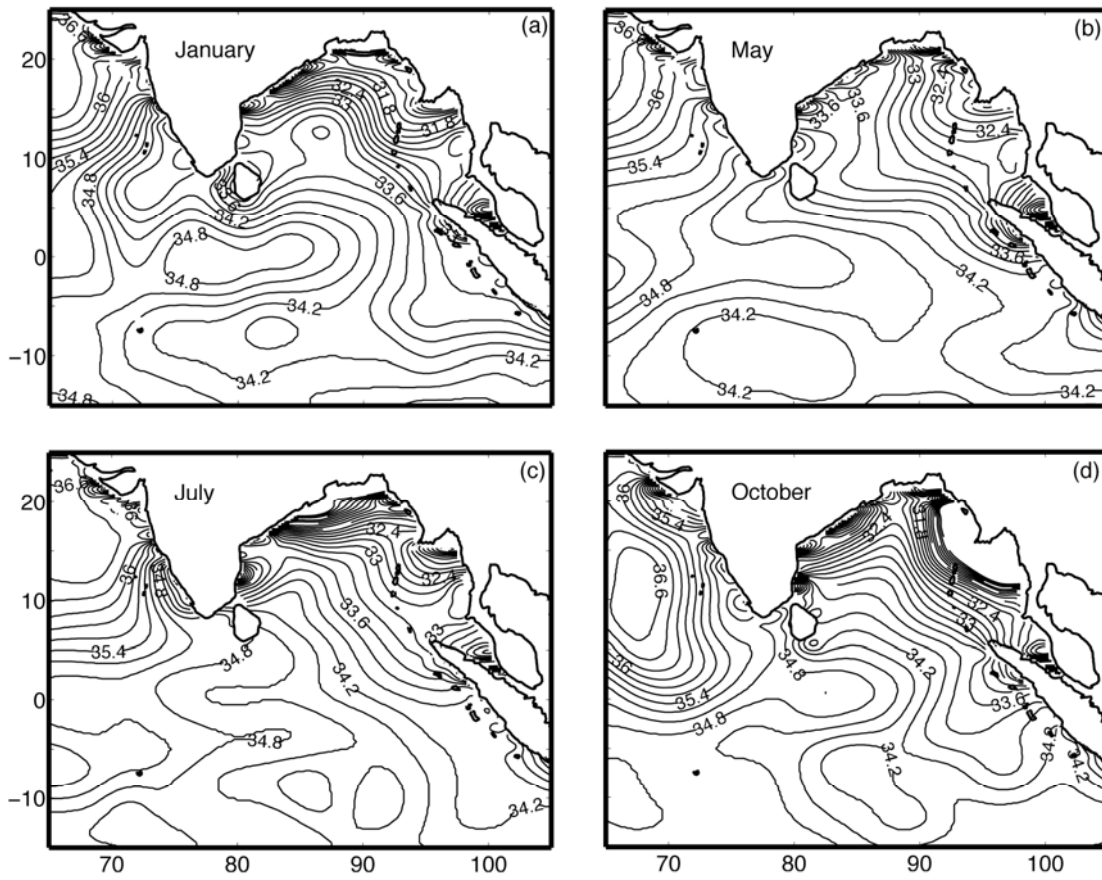


Figure 3. World Ocean Atlas 2005 (WOA05) climatological Sea Surface Salinity (SSS) during (a) January, (b) May, (c) July, and (d) October.

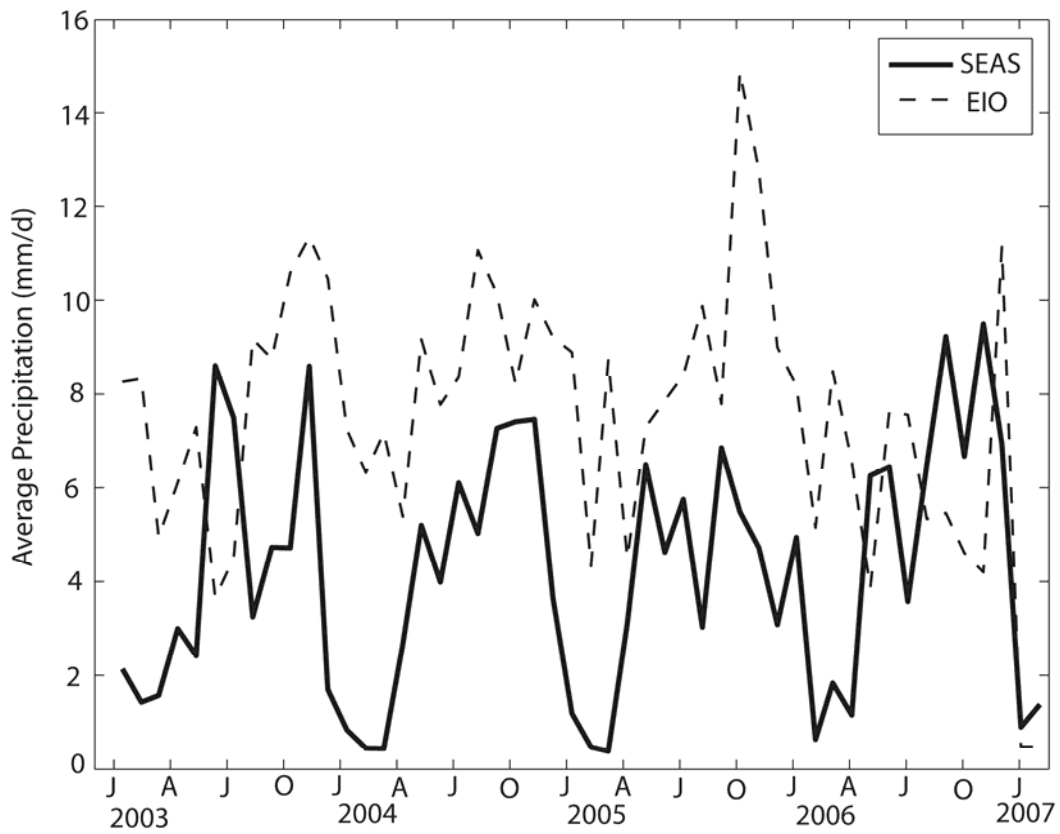


Figure 4. Interannual variation of rainfall obtained from the Global Precipitation Climatology Project (GPCP) in the EIO and SEAS during January 2003-February 2007.

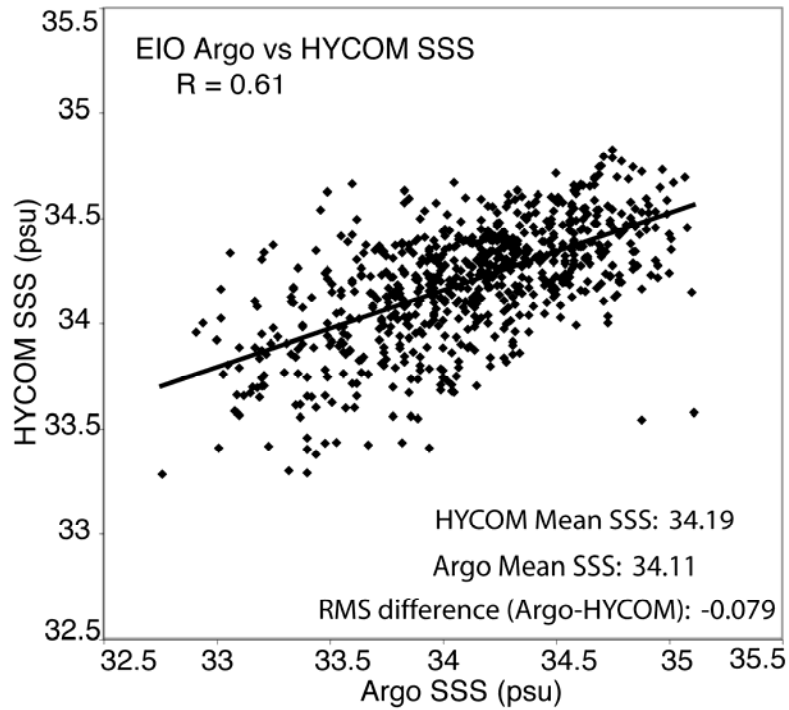


Figure 5. Scatter plot of Argo SSS and HYCOM SSS in the EIO box. The HYCOM output at each of the 10 day cycle location of the Argo float (s) in the EIO box during 2003-06. The correlation coefficient is 0.61.

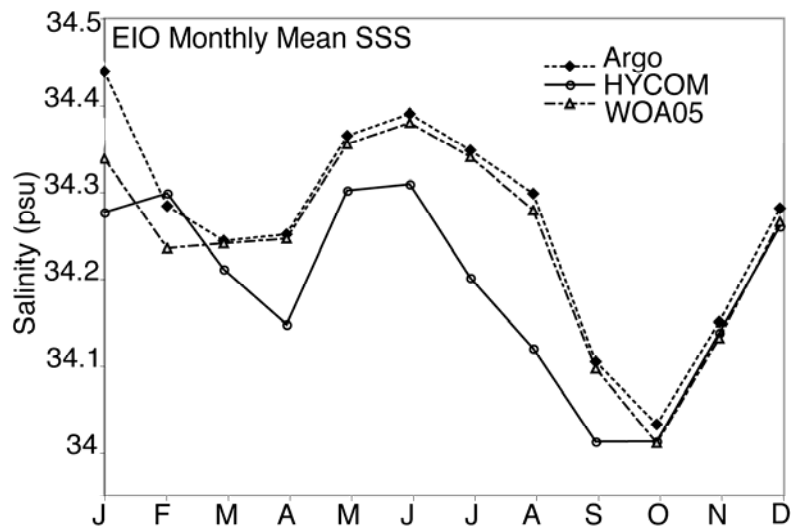


Figure 6. Annual variation of climatological (WOA05) SSS, Argo SSS and HYCOM SSS in the EIO box. The seasonal cycle of Argo SSS is based on the data from January 2002 to December 2006 and that of HYCOM SSS is based on data from January 2003 to December 2006.

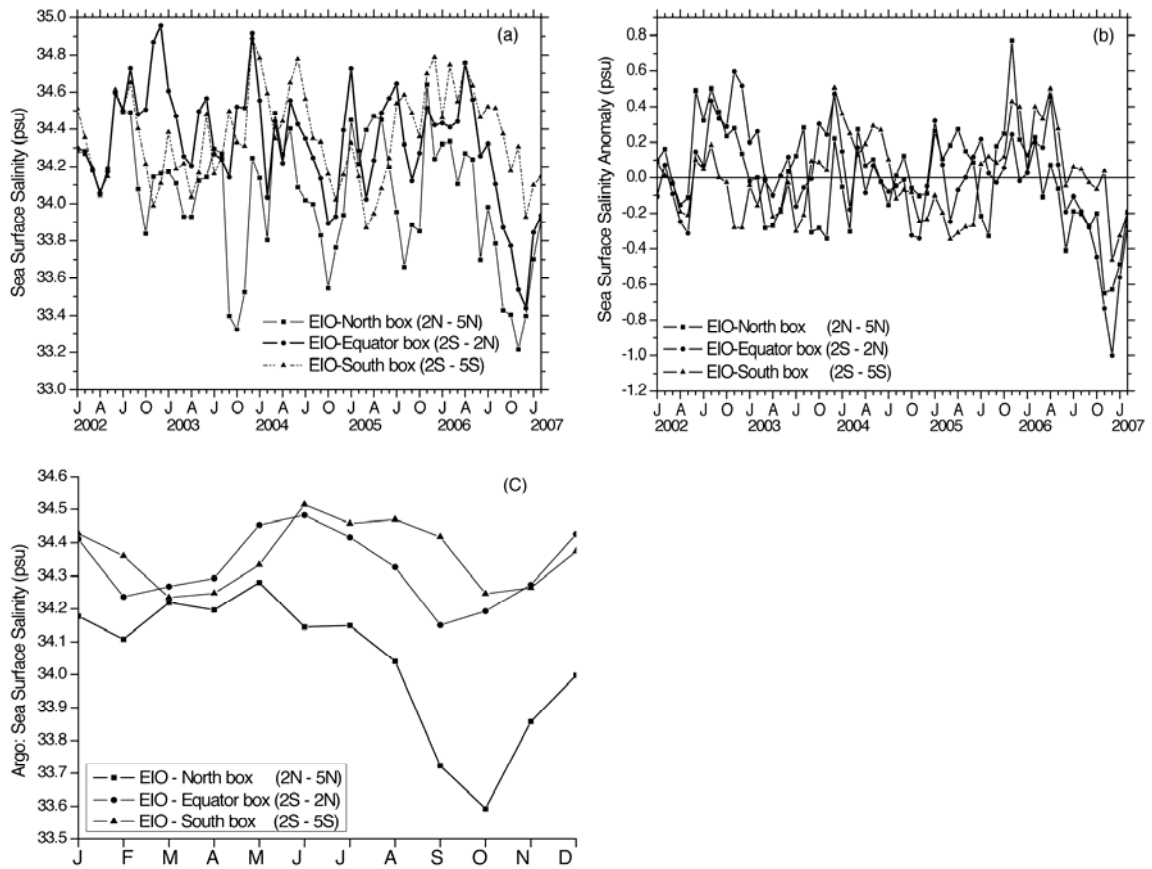


Figure 7. Interannual variation of (a) Argo sea surface salinity, (b) Argo sea surface salinity anomaly during January 2002 –February 2007 and (c) annual cycle of Argo sea surface salinity in each of the Equatorial boxes [EIO-north box, EIO-equator box, and EIO-south box]. The 5 year mean (2002-2006) annual cycle of Argo surface salinity (c) for each box is used to obtain the sea surface salinity Anomaly in each box.

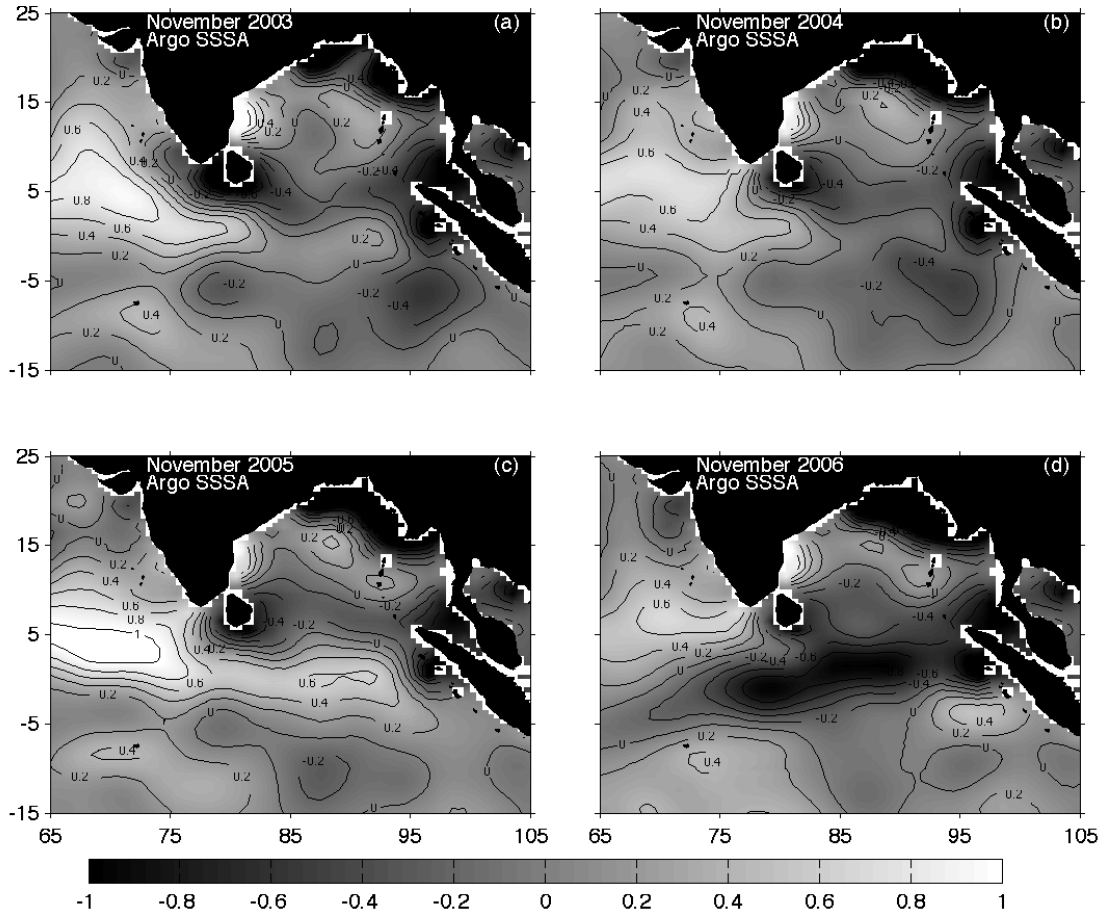


Figure 8. Spatial variations of monthly mean Argo SSSA for November in different years in the tropical Indian Ocean during (a) 2003, (b) 2004, (c) 2005 and (d) 2006.

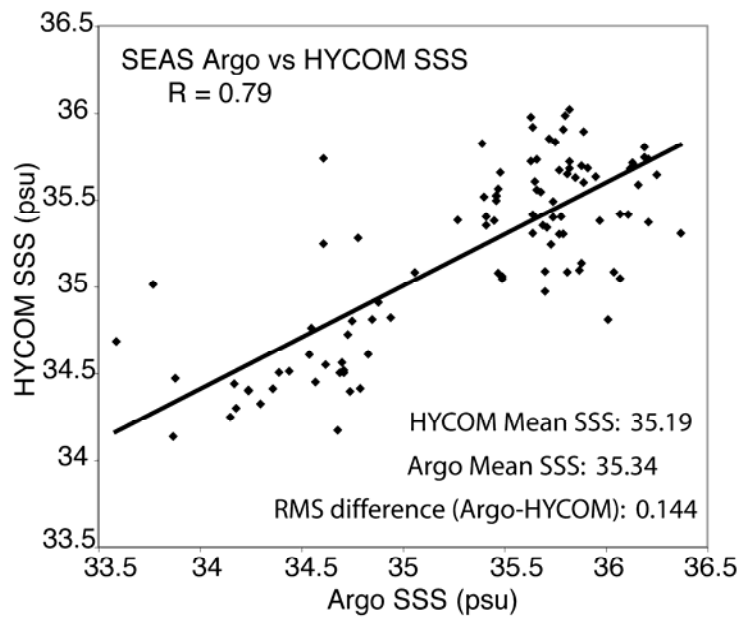


Figure 9. Scatter plot of Argo SSS and HYCOM SSS in the SEAS box. The HYCOM SSS output plotted at each of the 10 day cycle location of the Argo float(s) in the SEAS box during May 2004-October 2005. The correlation coefficient (r) is 0.79

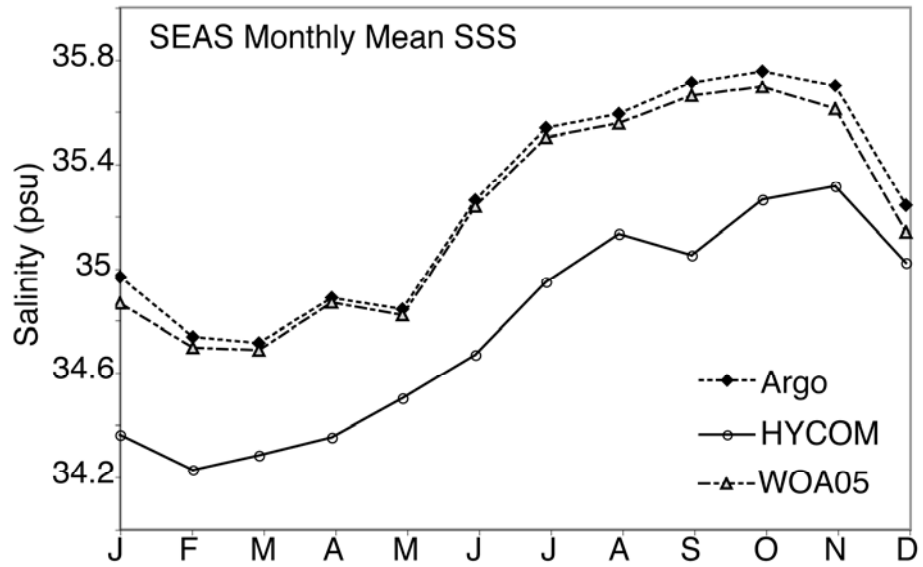


Figure 10. Annual variation of Argo SSS, HYCOM SSS and climatological (WOA05) SSS in the SEAS box.

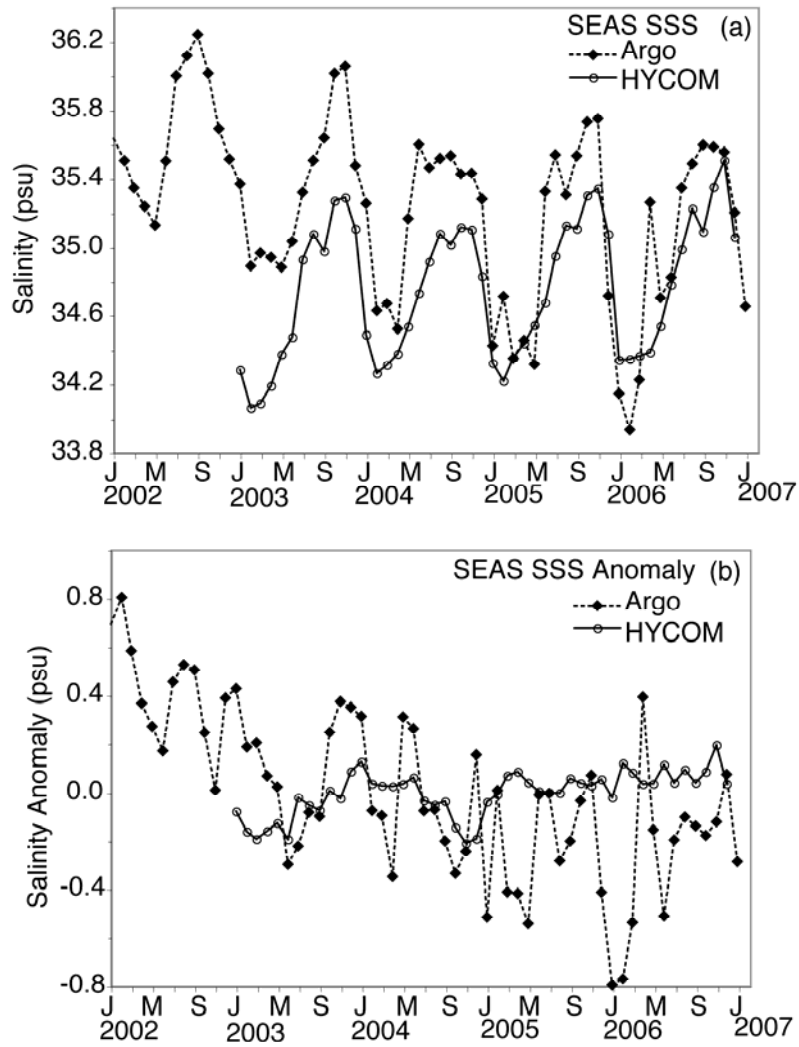


Figure 11. Interannual variation of (a) Argo SSS (dotted line) and HYCOM SSS (solid line), and (b) Argo and HYCOM SSSA in the SEAS box during January 2002-January 2007

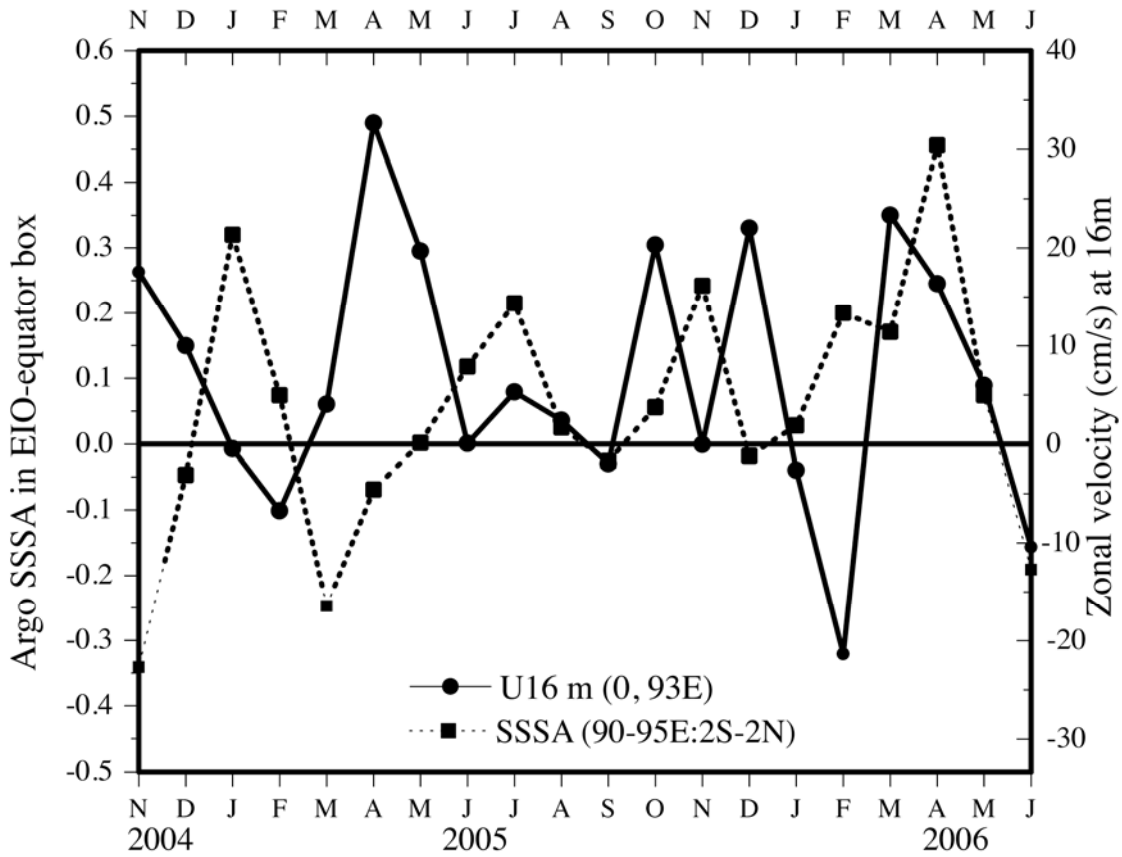


Figure 12. Acoustic Doppler Current Profiler (ADCP) measured monthly mean zonal velocity (cm/s) at 16 m depth (solid line) at 0°, 93°E and Argo SSSA (dashed line) in the EIO-equator box during November 2004 – July 2006.

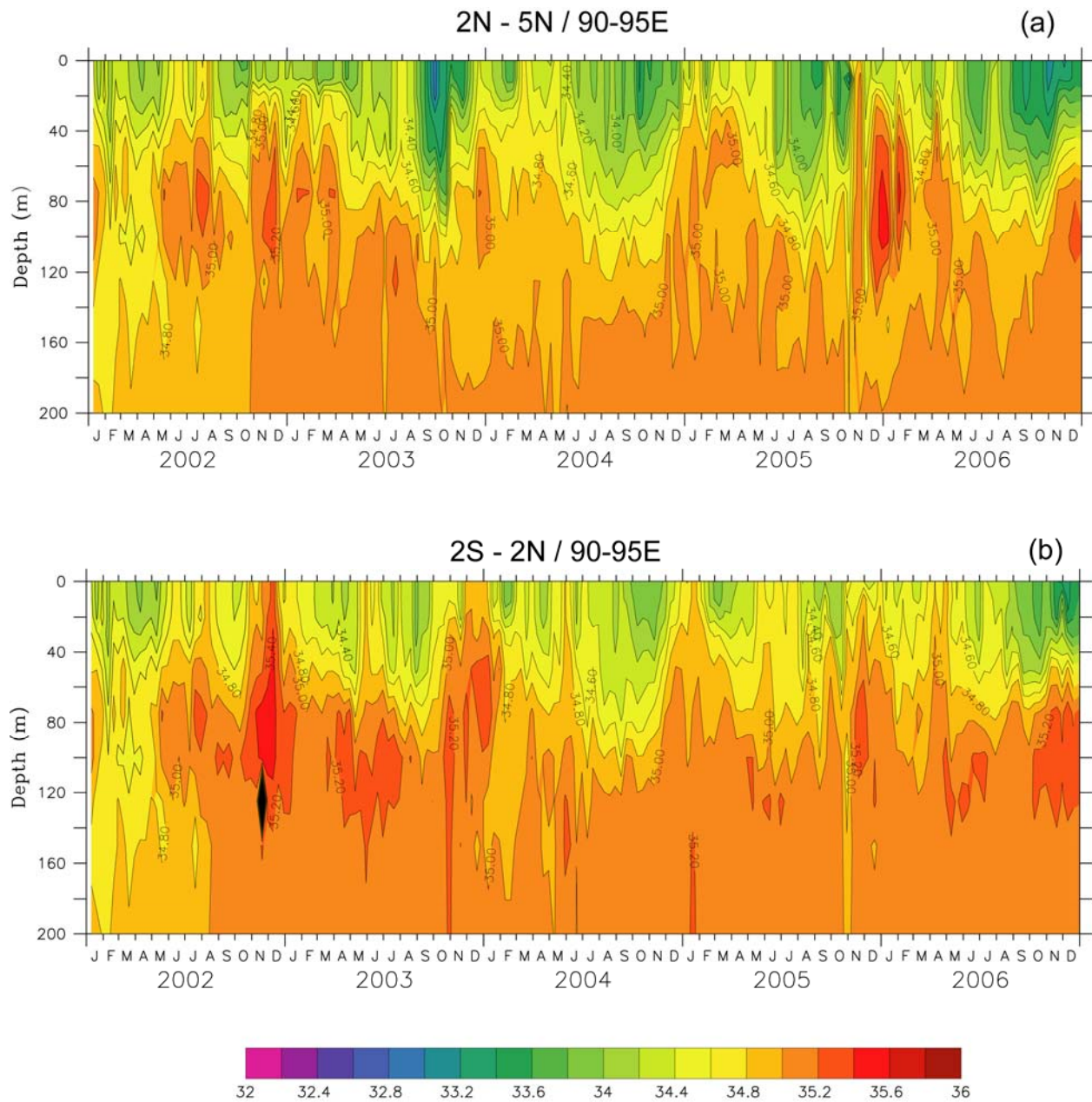


Figure 13. Interannual variation of Argo Salinity structure in the upper 200 m in the (a) EIO-north box (2°N - 5°N , 90° - 95°E) and (b) EIO-equator box (2°S - 2°N , 90° - 95°E) during 2002-2006.

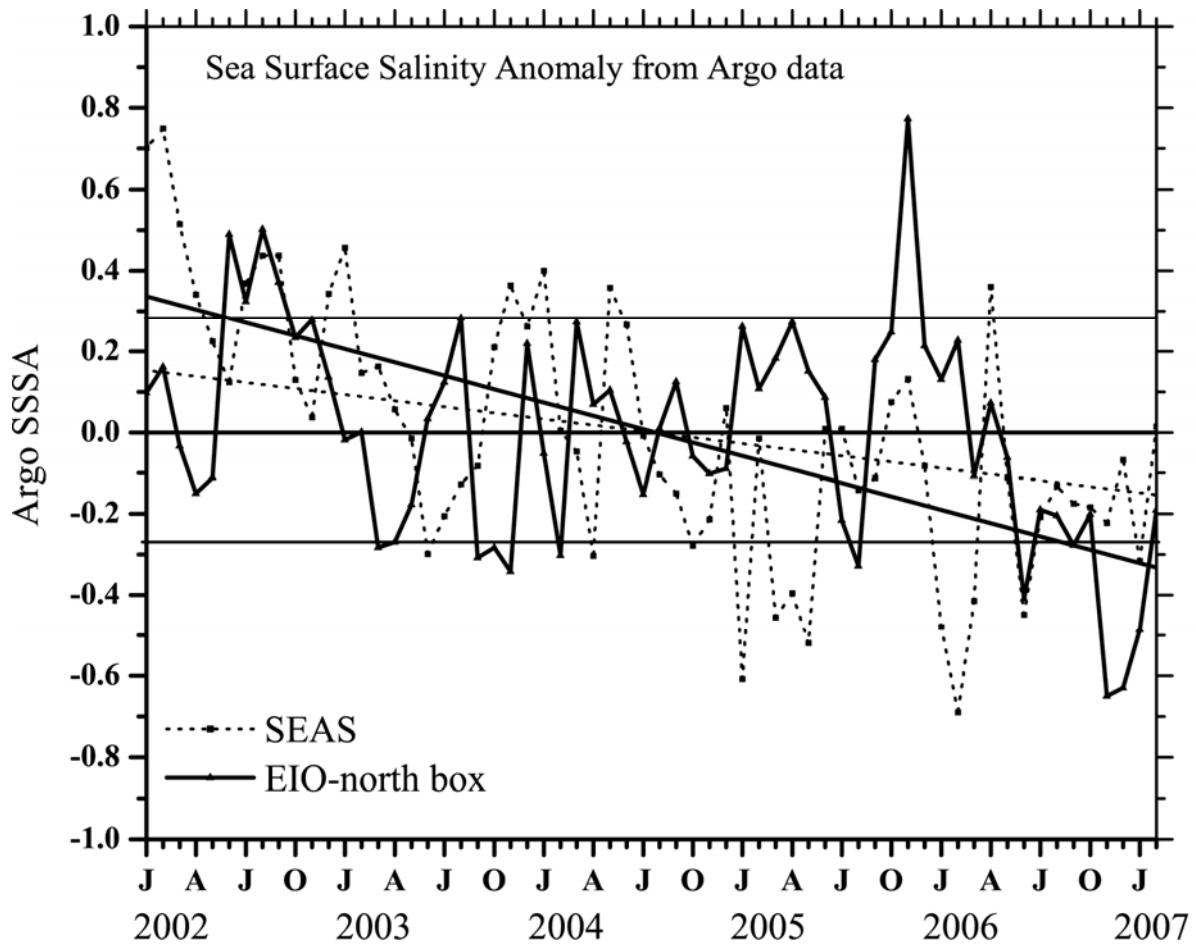


Figure 14. Interannual variation of Argo SSSA in the EIO-north box and SEAS box during January 2002 – February 2007. Standard deviation for both data sets is the same and is shown by horizontal lines. Linear trend lines fitted for SSSA variation in each box are also shown.

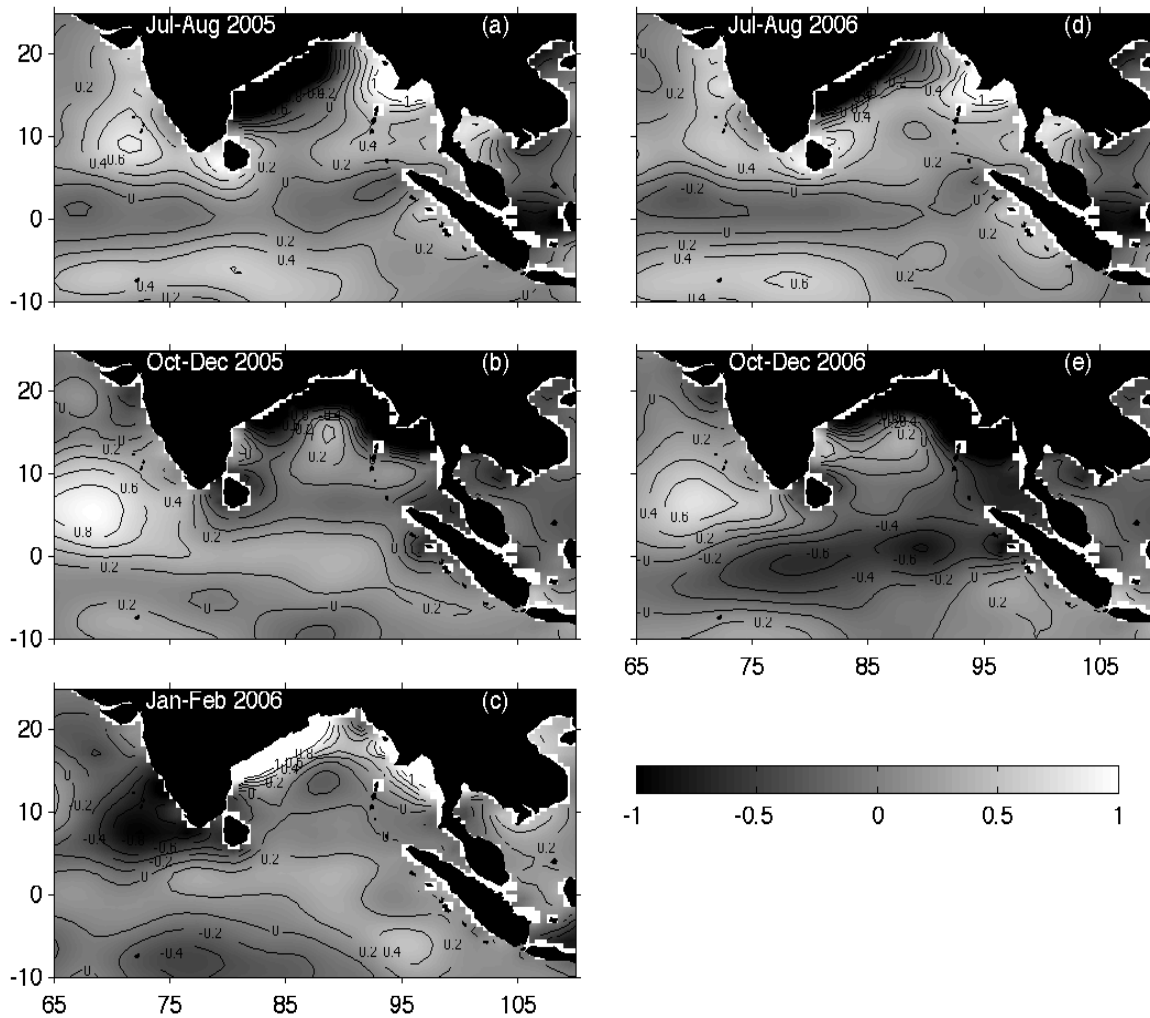


Figure 15. Spatial variation of gridded Argo SSSA (obtained after subtracting the 5 year (2002-2006) mean seasonal cycle) for the selected periods (a & d) prior to IODZM event (July-August), (b & e) during the IODZM event (October – December), (c) after the negative IODZM event (January – February 2006).

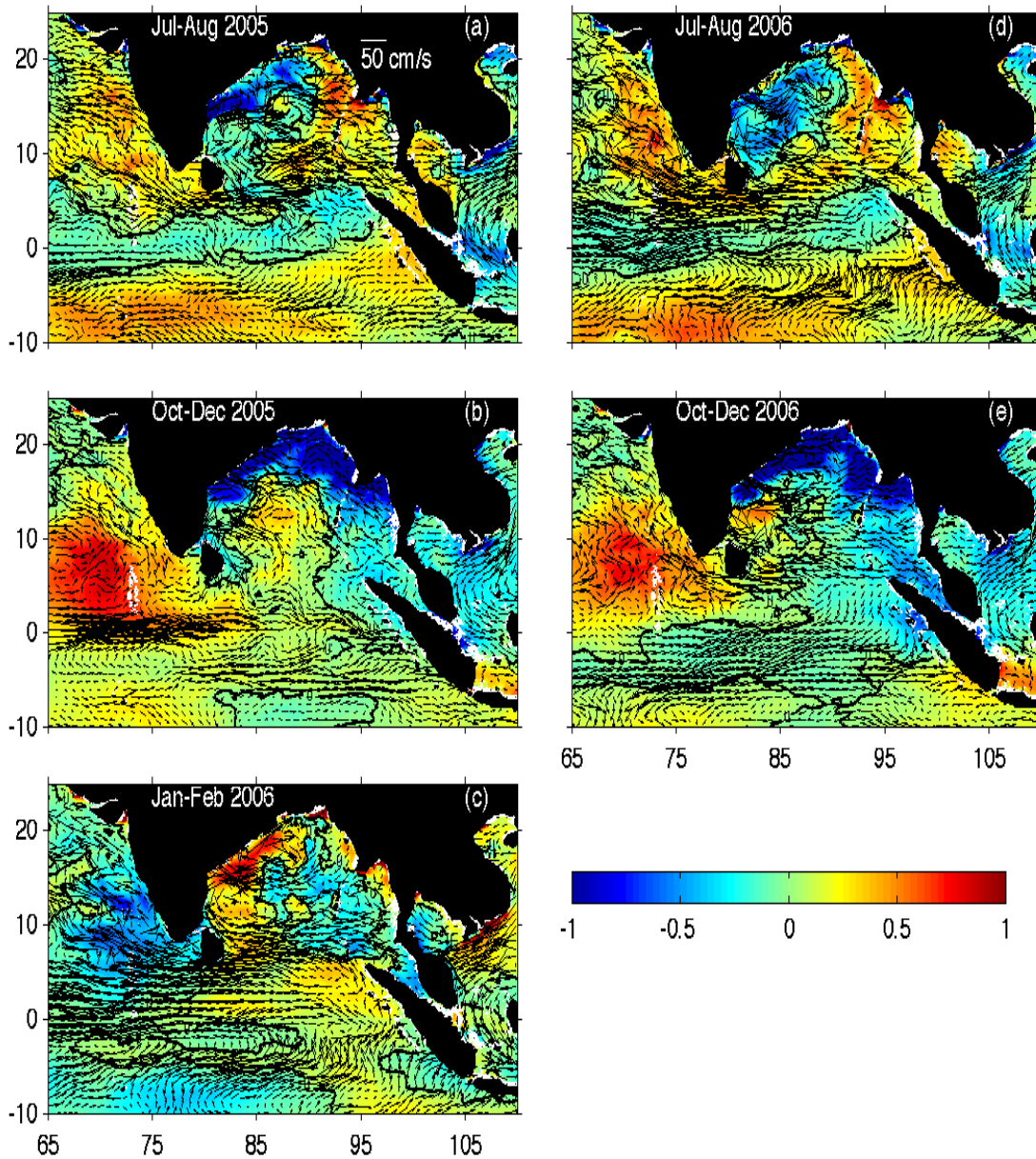


Figure 16. HYCOM simulations of Sea Surface Salinity Anomaly (color shading) and current vectors anomaly for the selected periods of (a & d) prior to IODZM event (July-August), (b & e) during the IODZM event (October – December), (c) after the negative IODZM event (January – February 2006). The 4 years (2003-2006) mean seasonal cycle is subtracted to obtain the anomalies in the model surface salinity and surface currents.

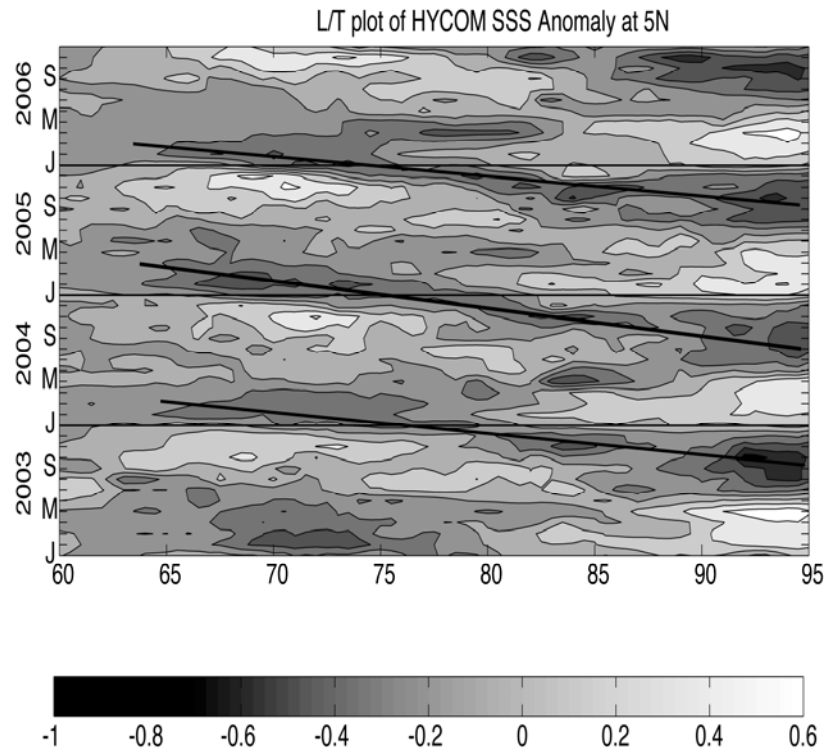


Figure 17. Longitude-Time plot of HYCOM SSSA in the southern Bay of Bengal along 5°N latitude during 2003-2006.